Consistent section-averaged shallow water equations with bottom friction

Victor Michel-Dansac, Pascal Noble, Jean-Paul Vila

Consistent section-averaged shallow water equations with bottom friction

Victor Michel-Dansac, Pascal Noble, Jean-Paul Vila *

December 19, 2018

Abstract. In this paper, we present a general framework to construct section-averaged models when the flow is constrained – e.g. by topography – to be almost one-dimensional. These models are consistent with the two-dimensional shallow water equations. After rewriting the two-dimensional shallow water equations in a suitable set of coordinates allowing to take care of a meandering configuration, we consider the quasi one-dimensional regime. Then, we expand the water elevation and velocity field in the spirit of the diffusive wave equations and establish a set of one-dimensional equations made of a mass, momentum and energy equations which are close to the ones usually used in hydraulic engineering. Our model reduces to classical shallow water models with variable sections found in the literature. Out of these configurations, there is an $\mathcal{O}(1)$ deviation of our model from the classical ones. Finally, we present the main mathematical properties of our model and carry out numerical simulation as validation of our approach with comparison to the full two-dimensional shallow water equations.

1 Introduction

In environmental modeling of free surface flows, the "shallow water" models are often used in order to reduce the complexity of the full Navier-Stokes equations and to reduce the computational cost implied by numerically solving such three-dimensional free surface flow equations. Such systems are commonly found in the simulation of various geophysical phenomena such as rivers, coastal flows, floods [Marin and Monnier, 2009], and they are standard models in hydraulics. The mathematical derivation of such models is now well-documented in many situations, under the assumption that the section of the channel is rectangular. For instance, see [Richard et al., 2017] and [Bresch and Noble, 2007] in the context of respectively turbulent and laminar flows, and see [Dammuller et al., 1989] in the context of meander flows where the 2D shallow water equations are derived formally and numerical simulations are carried out under the assumption that sedimentation is neglected.

We will focus in this paper in this particular regime of fixed topographies, which do not depend on time. However, in order to simplify equations and reduce computational efforts to solve the full two-dimensional shallow water equations, we will consider the section-averaged shallow water equations. These models are of particular interest in hydraulic engineering due to their simplicity and reduced computational cost. The river is supposed to flow in the presence of meanders and the cross section is variable. The shallow water system derived in this context reads as follows [Marin and Monnier, 2009, Decoene et al., 2009]:

$$\begin{cases} S_t + Q_{\xi_1} = 0, \\ Q_t + \left(\beta \dfrac{Q^2}{S}\right)_{\xi_1} + \dfrac{S H_{\xi_1}}{F^2} = \dfrac{J_0}{\varepsilon F^2} S \left(\mathcal{I} - \dfrac{Q|Q|}{H^{2+p} c_{SW}^2}\right), \end{cases} \tag{1.1}$$

*Institut de Mathématiques de Toulouse; UMR5219, Université de Toulouse; CNRS, INSA, F-31077, France; victor.michel-dansac@math.univ-toulouse.fr, noble@math.univ-toulouse.fr, vila@insa-toulouse.fr

where c_{SW} is some friction coefficient and β is the so-called Boussinesq term, which is equal to 1 if the flow is one-dimensional (i.e. constant in the cross-stream direction). When $\beta \neq 1$, the shallow water model is no longer Euclidean-invariant. Moreover, the meandering aspect was not considered in [Marin and Monnier, 2009, Decoene et al., 2009]. It is our purpose to address the question of deriving 1D consistent shallow water models in the presence of meanders and for arbitrary geometries of the channel.

The paper is organized as follows. In section 2, we introduce the 2D shallow water model, which we consider as the exact model for the flow of a meandering river. We write this system in a set of curvilinear coordinates in order to describe meandering. Then, in order to write a simplified 1D model, we introduce several scaling assumptions and perform a non-dimensionalization of the 2D shallow water system, which is then averaged across the width of the channel. Section 3 is dedicated to carrying out asymptotic expansions of the fluid velocity and pressure field in the one-dimensional limit in order to close the averaged shallow water equations. In section 4, in the strongly meandering case, we build a zeroth-order shallow water model: the friction term is built so as to ensure the consistency of the discharge rate to the main order. The structure is very simple, completely similar to the section-averaged shallow water models found in the literature (see e.g. [Decoene et al., 2009]). In section 5, we propose our new model and analyze its mathematical structure in the case of weakly meandering channels. It is a four-equation model describing the evolution of the wetted surface, the discharge rate, the energy and an additional quantity, called "enstrophy", which accounts for the vorticity of the flow in the cross-stream direction. This new model provides a first-order accurate description of the surface elevation, the discharge rate, and the energy; in addition, it is hyperbolic. The last section of this paper is dedicated to a numerical validation of our model. We compare the accuracy of three section-averaged models: the two (zeroth- and first-order) models we derived in this paper and a section-averaged shallow water model simply obtained by assuming that the downstream velocity is constant across the channel section (and which is obviously non consistent for channels that are not U-shaped).

Perspectives. In this paper, we have restricted our attention to fixed topographies. It is of particular interest to consider this type of model in the presence of sedimentation. It is of particular interest to consider this type of model in the presence of sedimentation. In [Odgaard, 1989a, Odgaard, 1989b], such a problem was considered for stationary flows in order to determine the mechanisms of migration of meanders. A model was formally derived and the study was completed with various numerical simulations. However, the asymptotic analysis was conducted with non consistent assumptions on the velocity profile. A non-stationary model with sedimentation was derived in [Chen and Duan, 2006] but for channels with vertical walls. We expect that our approach can be extended to transport of sediments in channels with arbitrary cross sections in a similar way. Another problem of interest is the coupling between 1D and 2D shallow water models: the aim here is either to carry out a complete modeling of an estuary or to model river floods, see e.g. [Fernández-Nieto et al., 2010] for the setting of the latter. Our model is built directly from the 2D shallow water equations, which ensures a natural coupling between the two models.

2 Governing equations

In this section, we consider the two-dimensional shallow water equations with bottom friction

$$\begin{cases} h_t + \mathrm{div}_{\mathbf{X}}(h\mathbf{u}) = 0, \\ \mathbf{u}_t + \mathbf{u}.\boldsymbol{\nabla}_{\mathbf{X}}\mathbf{u} + g\boldsymbol{\nabla}_{\mathbf{X}}h = g\left(-\boldsymbol{\nabla}_{\mathbf{X}}Z - \dfrac{\mathbf{u}\|\mathbf{u}\|}{C_h^2\, h^p}\right), \end{cases} \tag{2.1}$$

where g is the gravity constant, h the fluid height, $\mathbf{u} = (u_1, u_2) \in \mathbb{R}^2$ the fluid velocity and C_h^2 is the Chézy friction coefficient. The unknowns h and $\mathbf{u}$ depend on the time variable t and the space variable $\mathbf{X} = (x_1, x_2) \in \mathbb{R}^2$. For the sake of simplicity, we have chosen a simple friction law that depends only on the fluid height. We could also have considered more realistic formulas for the bottom friction τ_b, by including the hydraulic radius,

like the Chézy formula

$$\tau_b = -\frac{\mathbf{u}\|\mathbf{u}\|}{C^2 R_h},$$

where C^2 is the Chézy friction term and R_h is the hydraulic radius. An alternative is the Manning-Strickler formula

$$\tau_b = -\frac{\mathbf{u}\|\mathbf{u}\|}{K^2 R_h^{4/3}}, \quad K = \frac{C^2}{R_h^{1/6}}.$$

Note that other formulas were derived in various situations, e.g. triangular, trapezoidal, or circular channels, to get complicated forms of the bottom friction valid mostly for stationary flows [Zarrati et al., 2008, Zaghloul, 1998]. In what follows, we will assume that the friction coefficient C_h depends on $\mathbf{X}$. The system (2.1) admits an additional energy balance law:

$$(E_{2D})_t + \mathrm{div}_{\mathbf{X}}\left(\mathbf{u}\left(E_{2D} + \frac{1}{2}gh^2\right)\right) = gh\left(-\mathbf{u}.\boldsymbol{\nabla}_{\mathbf{X}} Z - \frac{\|\mathbf{u}\|^3}{C_h^2 h^p}\right).$$

where the energy E_{2D} is given by $E_{2D} = \frac{h}{2}\|\mathbf{u}\|^2 + g\frac{h^2}{2}$. This equation can also be rewritten with a negative source term:

$$(E_{2D} + ghZ)_t + \mathrm{div}_{\mathbf{X}}\left(\mathbf{u}\left(E_{2D} + ghZ + \frac{1}{2}gh^2\right)\right) = -gh\frac{\|\mathbf{u}\|^3}{C_h^2 h^p}.$$

We now write the system (2.1) in a reference frame which fits with the geometry of the channel. In order to study the limit of quasi one-dimensional flows, we write the new system in a non-dimensional form together with its exact section-averaged version.

2.1 Parameterization of the problem

In order to deal with the meanders of the river, we now introduce a parameterization of the river bed: for that purpose, we assume that it follows a parameterized curve $\mathbf{r} : \xi_1 \mapsto (\bar{x}(\xi_1), \bar{y}(\xi_1))$ such that $\bar{x}'(\xi_1)^2 + \bar{y}'(\xi_1)^2 = 1$, see Figure 1. We naturally introduce the Frenet reference frame:

$$(\bar{x}'(\xi_1), \bar{y}'(\xi_1)) = (\cos(\theta(\xi_1)), \sin(\theta(\xi_1))) := \mathbf{T}(\xi_1), \quad \mathbf{N}(\xi_1) = (-\sin(\theta(\xi_1)), \cos(\theta(\xi_1))).$$

Recall the classical relation, which also defines the curvature radius $R(\xi_1)$:

$$\frac{d\mathbf{T}}{d\xi_1} = \theta'(\xi_1)\mathbf{N}(\xi_1) := \frac{1}{R(\xi_1)}\mathbf{N}(\xi_1), \qquad \text{i.e.} \quad R(\xi_1) = \frac{1}{\theta'(\xi_1)}.$$

We now introduce the bijective change of variables from the Euclidean space to the Frenet reference frame. A point $\boldsymbol{\xi} = (\xi_1, \xi_2)$ of the Frenet reference frame transforms into a point $\mathbf{X} = (x_1, x_2)$ of the Euclidean space according to $\mathbf{X}(\xi_1, \xi_2) = \mathbf{r}(\xi_1) + \xi_2\mathbf{N}(\xi_1)$. In what follows, we introduce the bijective change of variables $\boldsymbol{\xi} = a(\mathbf{X})$ from the Euclidean space to the Frenet reference frame, whose inverse function is defined by

$$a^{-1}(\xi_1, \xi_2) = \begin{pmatrix} x_1(\xi_1, \xi_2) \\ x_2(\xi_1, \xi_2) \end{pmatrix} = \begin{pmatrix} \bar{x}(\xi_1) - \xi_2 \sin(\theta(\xi_1)) \\ \bar{y}(\xi_1) + \xi_2 \cos(\theta(\xi_1)) \end{pmatrix}.$$

In this reference frame, we assume that the bottom topography is parameterized by (see Figure 2)

$$Z(x_1(\xi_1, \xi_2), x_2(\xi_1, \xi_2)) = b_0(\xi_1) + \phi(\xi_1, \xi_2), \quad \phi(\xi_1, 0) = 0, \quad \forall \xi_1 \in \mathbb{R}.$$

Now, we rewrite the shallow water equation system (2.1) in this new set of coordinates. For that purpose, we denote by

$$\mathcal{F}(\xi_1, \xi_2) := A^{-1}(\xi_1, \xi_2) = \begin{pmatrix} \cos(\theta(\xi_1))\left(1 - \dfrac{\xi_2}{R(\xi_1)}\right) & -\sin(\theta(\xi_1)) \\ \sin(\theta(\xi_1))\left(1 - \dfrac{\xi_2}{R(\xi_1)}\right) & \cos(\theta(\xi_1)) \end{pmatrix}$$

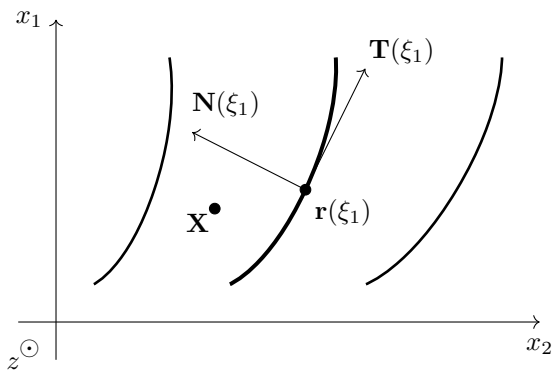

Figure 1: Sketch of a meandering river viewed from above, and notations.

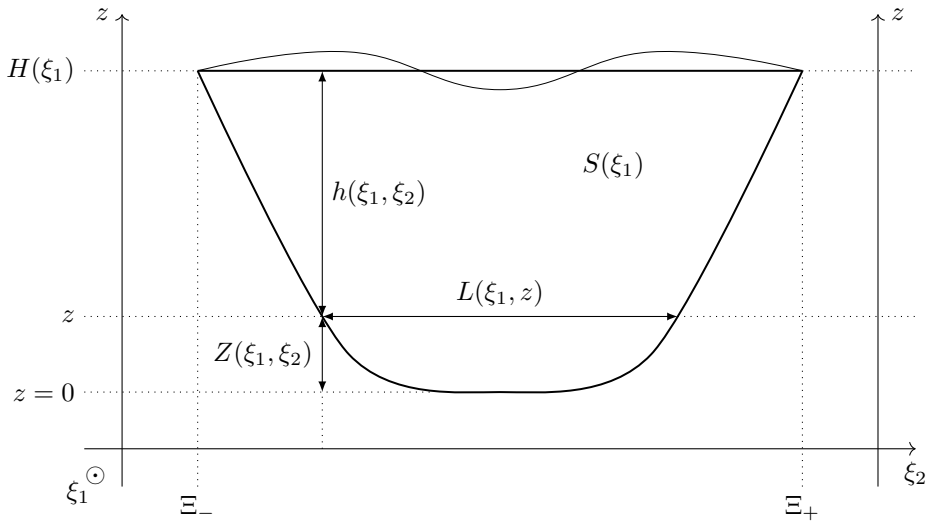

Figure 2: Sketch of a section of the channel geometry and additional notations.

the Jacobian matrix of the change of variables $a^{-1}(\xi_1,\xi_2)$ defined above. We also set

$$|\mathcal{F}| := \det(\mathcal{F}) = 1 - \frac{\xi_2}{R(\xi_1)}.$$

We introduce the fluid velocity $\mathbf{v}$ in the Frenet frame, defined by $\mathbf{u} = \mathcal{F}(\xi_1,\xi_2)\mathbf{v}$. We denote by $A(x_1,x_2)$ the Jacobian matrix of the change of variables $a(x_1,x_2)$. We then have the following chain rules:

Lemma 2.1 *For any vector fields* $\mathbf{z}$ *and* $\mathbf{v} = A\mathbf{u}$*, the differential operators transform according to*

$$|\mathcal{F}|\mathrm{div}_{\mathbf{X}}(\mathbf{z}) = \mathrm{div}_{\boldsymbol{\xi}}(|\mathcal{F}|A\mathbf{z}), \quad \mathbf{u}.\boldsymbol{\nabla}_{\mathbf{X}} = \mathbf{v}.\boldsymbol{\nabla}_{\boldsymbol{\xi}}, \quad \boldsymbol{\nabla}_{\mathbf{X}} = A^T\boldsymbol{\nabla}_{\boldsymbol{\xi}}.$$

Let us rewrite (2.1) in this new system of coordinates. We first consider the mass conservation law. According to Lemma 2.1, we get:

$$|\mathcal{F}|h_t = -|\mathcal{F}|\mathrm{div}_{\mathbf{X}}(h\mathbf{u}) = -\mathrm{div}_{\boldsymbol{\xi}}(|\mathcal{F}|A\mathbf{u}) = -\mathrm{div}_{\boldsymbol{\xi}}(|\mathcal{F}|h\mathbf{v}).$$

We introduce the notation $\tilde{h} = |\mathcal{F}|h$. The mass conservation law in this new system of coordinates reads

$$\tilde{h}_t + \mathrm{div}_{\boldsymbol{\xi}}\,(\tilde{h}\mathbf{v}) = 0.$$

Let us now consider the discharge balance law. Using Lemma 2.1, we get

$$\mathbf{v}_t + A\mathbf{v}.\boldsymbol{\nabla}_{\boldsymbol{\xi}}\left(A^{-1}\mathbf{v}\right) + g\,AA^T\boldsymbol{\nabla}_{\boldsymbol{\xi}}\left(h+Z\right) = -\frac{g|A^{-1}\mathbf{v}|}{C_h^2 h^p}\mathbf{v}.$$

It is easily shown that $AA^T = \mathrm{diag}(|\mathcal{F}|^{-2}, 1)$ and

$$A\mathbf{v}.\boldsymbol{\nabla}_{\boldsymbol{\xi}}\left(A^{-1}\mathbf{v}\right) = \mathbf{v}.\boldsymbol{\nabla}_{\boldsymbol{\xi}}\mathbf{v} + \Gamma(\mathbf{v}), \quad \text{where } \Gamma(\mathbf{v}) = \begin{pmatrix} \dfrac{v_1^2}{R(\xi_1)}\dfrac{\xi_2 R'(\xi_1)}{R(\xi_1)-\xi_2} - \dfrac{v_1 v_2}{R(\xi_1)}\dfrac{2R(\xi_1)}{R(\xi_1)-\xi_2} \\ \dfrac{v_1^2}{R(\xi_1)}\dfrac{R(\xi_1)-\xi_2}{R(\xi_1)} \end{pmatrix}.$$

The additional term Γ represents centripetal forces. In this new reference frame, the shallow water system reads:

$$\begin{cases} \tilde{h}_t + (\tilde{h}v_1)_{\xi_1} + (\tilde{h}v_2)_{\xi_2} = 0, \\ (v_1)_t + v_1(v_1)_{\xi_1} + v_2(v_1)_{\xi_2} + \dfrac{v_1^2}{R(\xi_1)}\dfrac{\xi_2 R'(\xi_1)}{|\mathcal{F}|R(\xi_1)} - \dfrac{2v_1v_2}{|\mathcal{F}|R(\xi_1)} + \dfrac{g}{|\mathcal{F}|^2}(h+Z)_{\xi_1} = -\dfrac{gv_1}{C_h^2 h^p}\sqrt{|\mathcal{F}|^2 v_1^2 + v_2^2}, \\ (v_2)_t + v_1(v_2)_{\xi_1} + v_2(v_2)_{\xi_2} + |\mathcal{F}|\dfrac{v_1^2}{R(\xi_1)} + g(h+Z)_{\xi_2} = -\dfrac{gv_2}{C_h^2 h^p}\sqrt{|\mathcal{F}|^2 v_1^2 + v_2^2}. \end{cases} \tag{2.2}$$

The energy equation reads, in that setting,

$$(|\mathcal{F}|E_{2D})_t + \mathrm{div}_{\vec{\xi}}\left(|\mathcal{F}|\mathbf{v}\left(E_{2D} + \frac{1}{2}gh^2\right)\right) = g\tilde{h}\left(-\mathbf{v}.\boldsymbol{\nabla}Z - \frac{|A^{-1}\mathbf{v}|^3}{C_h^2\,h^p}\right),$$

or, equivalently,

$$\left(|\mathcal{F}|(E_{2D}+ghZ)\right)_t + \mathrm{div}_{\boldsymbol{\xi}}\left(|\mathcal{F}|\mathbf{v}\left(E_{2D}+ghZ+\frac{1}{2}gh^2\right)\right) = -g\tilde{h}\frac{|A^{-1}\mathbf{v}|^3}{C_h^2\,h^p}.$$

2.2 Non-dimensional form of the system

Next, in order to study the quasi one-dimensional flow limit, we write the system (2.2) in a non-dimensional form. For that purpose, we introduce the following scales:

$$v_1 := \mathcal{U}v_1 \quad v_2 := \mathcal{V}v_2, \quad h := \mathcal{H}h, \quad \xi_1 := \mathcal{X}\xi_1, \quad \xi_2 := \mathcal{Y}\xi_2,$$

where $\mathcal{U}$ is the typical fluid velocity in the downstream direction whereas $\mathcal{V}$ is the typical fluid velocity in the cross-stream direction. The height $\mathcal{H}$ represents the typical fluid height, whereas $\mathcal{Y}$ is the typical channel width and $\mathcal{X}$ is a characteristic wavelength. We also introduce the typical time scale $\mathcal{T} = \mathcal{X}/\mathcal{U}$. The non-dimensional mass conservation law then reads

$$(|\mathcal{F}|h)_t + (|\mathcal{F}|hv_1)_{\xi_1} + \frac{R_v}{R_l}(|\mathcal{F}|hv_2)_{\xi_2} = 0, \quad R_v = \frac{\mathcal{V}}{\mathcal{U}}, \quad R_l = \frac{\mathcal{Y}}{\mathcal{X}}.$$

In what follows, we assume $R_v = R_l$ in order to keep the mass conservation law unchanged. Furthermore, we suppose that $R_l \ll 1$, which is consistent with the quasi-one-dimensional setting. We also take $R := \mathcal{R}R$, where $\mathcal{R}$ is the typical curvature radius found in the meanders of the river, and we set $R_y = \mathcal{Y}/\mathcal{R}$. In that setting, we have

$$|\mathcal{F}| = 1 - \frac{R_y\xi_2}{R(\xi_1)}.$$

We finally scale the bottom topography and bottom friction as follows:

$$b_0 := \mathcal{B} b_0\left(\frac{\xi_1}{\mathcal{X}}\right), \quad \phi := \mathcal{H}\phi\left(\frac{\xi_1}{\mathcal{X}}, \frac{\xi_2}{\mathcal{Y}}\right), \quad C_h^2 = \mathcal{C}^2\left(1 + c\left(\frac{\xi_1}{\mathcal{X}}, \frac{\xi_2}{\mathcal{Y}}\right)\right)^2.$$

The non-dimensional form of the shallow water system (2.2) therefore reads:

$$\begin{cases} (|\mathcal{F}|h)_t + (|\mathcal{F}|hv_1)_{\xi_1} + (|\mathcal{F}|hv_2)_{\xi_2} = 0, & \text{(2.3a)} \\ (v_1)_t + v_1(v_1)_{\xi_1} + v_2(v_1)_{\xi_2} + \dfrac{R_y v_1}{|\mathcal{F}|R(\xi_1)}\left(\dfrac{\xi_2 R'(\xi_1)}{R(\xi_1)}v_1 - 2v_2\right) + \dfrac{1}{|\mathcal{F}|^2F^2}(h+\phi)_{\xi_1} & \\ \qquad = \dfrac{-1}{\varepsilon F^2}\left(\dfrac{I_0 b_0'}{|\mathcal{F}|^2} + \dfrac{J_0 v_1\sqrt{|\mathcal{F}|^2v_1^2 + R_l^2v_2^2}}{(1+c)^2h^p}\right), & \text{(2.3b)} \\ (v_2)_t + v_1(v_2)_{\xi_1} + v_2(v_2)_{\xi_2} + \dfrac{R_y}{R_l^2}|\mathcal{F}|\dfrac{v_1^2}{R(\xi_1)} + \dfrac{1}{R_l^2F^2}(h+\phi)_{\xi_2} = -\dfrac{J_0}{\varepsilon F^2}\dfrac{v_2}{(1+c)^2h^p}\sqrt{|\mathcal{F}|^2v_1^2 + R_l^2v_2^2}, & \text{(2.3c)} \end{cases}$$

where we have set

$$I_0 = \frac{\mathcal{B}}{\mathcal{X}}, \quad J_0 = \frac{\mathcal{U}|\mathcal{U}|}{\mathcal{C}^2\,\mathcal{H}^p}, \quad \varepsilon = \frac{\mathcal{H}}{\mathcal{X}}.$$

We write the last equation as

$$(h+\phi)_{\xi_2} + R_y|\mathcal{F}|F^2\frac{v_1^2}{R(\xi_1)} = -\frac{J_0R_l^2}{\varepsilon}\frac{v_2}{(1+c)^2h^p}\sqrt{|\mathcal{F}|^2v_1^2 + R_l^2v_2^2} - R_l^2F^2\Big((v_2)_t + v_1(v_2)_{\xi_1} + v_2(v_2)_{\xi_2}\Big). \quad (2.4)$$

The non-dimensional form of the energy is $E_{2D} = \dfrac{h}{2}\big(|\mathcal{F}|^2v_1^2 + R_l^2v_2^2\big) + \dfrac{h^2}{2F^2}$, and the energy equation reads

$$(|\mathcal{F}|E_{2D})_t + \mathrm{div}_{\tilde{\xi}}\left(|\mathcal{F}|\mathbf{v}\left(E_{2D} + \frac{h^2}{2F^2}\right)\right) = \frac{|\mathcal{F}|h}{\varepsilon F^2}\left(-I_0b_0'v_1 - \varepsilon\mathbf{v}.\boldsymbol{\nabla}_\xi\phi - J_0\frac{(|\mathcal{F}|^2v_1^2 + R_l^2v_2^2)^{3/2}}{(1+c)^2\,h^p}\right), \quad (2.5)$$

or, equivalently,

$$\left(|\mathcal{F}|\left(E_{2D} + \frac{h}{F^2}\left(\frac{I_0}{\varepsilon}b_0 + \phi\right)\right)\right)_t + \mathrm{div}_{\boldsymbol{\xi}}\left(|\mathcal{F}|\mathbf{v}\left(E_{2D} + \frac{h}{F^2}\left(\frac{I_0}{\varepsilon}b_0 + \phi + \frac{h}{2}\right)\right)\right)$$
$$= -J_0\frac{|\mathcal{F}|h}{\varepsilon F^2}\frac{(|\mathcal{F}|^2v_1^2 + R_l^2v_2^2)^{3/2}}{(1+c)^2\,h^p}.$$

2.3 Transverse averaging

Recall that the ultimate goal of these developments is to provide a suitable 1D section-averaged model to approximate the full 2D system (2.3). To that end, we need to write an average of the 2D system over the width of the channel. In what follows, we denote by $\Xi_-(\xi_1,t) < \Xi_+(\xi_1,t)$ the positions of the edges of the river. Either the channel is walled, and the river sides are the same as the given channel sides, or the channel does not have walls, like in Figure 2. In this second case, Ξ_- and Ξ_+ are defined implicitly as solutions of

$$h(\xi_1, \Xi_-(\xi_1,t), t) = 0, \qquad h(\xi_1, \Xi_+(\xi_1,t), t) = 0, \quad \forall t > 0, \quad \forall \xi_1 \in \mathbb{R}.$$

These are smooth functions of ξ_1 and t as long as $\phi_{\xi_2}(\xi_1, \Xi_\pm(\xi_1,t)) \neq 0$. This assumption is satisfied in the usual channels, for instance those with a trapezoidal or a triangular section. From now on, we consider this assumption to be satisfied. As a consequence, averaging the 2D system across the width of the channel consists in integrating the governing 2D equations between Ξ_- and Ξ_+.

We now apply this integration procedure to the equations (2.3a), (2.3b) (multiplied by $\tilde{h}$) and (2.5), i.e. the mass, x-discharge and energy equations of the non-dimensional 2D shallow water equations, to get:

$$\begin{cases} S_t + Q_{\xi_1} = 0, & \text{(2.6a)} \\ Q_t + \left(\displaystyle\int_{\Xi_-}^{\Xi_+} \tilde{h} v_1^2 \, d\xi_2\right)_{\xi_1} + \frac{1}{F^2} \int_{\Xi_-}^{\Xi_+} \frac{\tilde{h}}{|\mathcal{F}|^2} (h+\phi)_{\xi_1} \, d\xi_2 + \frac{R_y}{R(\xi_1)} \int_{\Xi_-}^{\Xi_+} h v_1 \left(\xi_2 v_1 \frac{R'(\xi_1)}{R(\xi_1)} - 2 v_2\right) d\xi_2 & \\ \qquad = -\frac{I_0}{\varepsilon F^2} \displaystyle\int_{\Xi_-}^{\Xi_+} \frac{\tilde{h}}{|\mathcal{F}|^2} b_0' \, d\xi_2 - \frac{J_0}{\varepsilon F^2} \int_{\Xi_-}^{\Xi_+} \frac{|\mathcal{F}| v_1 \sqrt{|\mathcal{F}|^2 v_1^2 + R_l^2 v_2^2}}{(1+c)^2 h^{p-1}} \, d\xi_2, & \text{(2.6b)} \\ \left(\displaystyle\int_{\Xi_-}^{\Xi_+} |\mathcal{F}| E \, d\xi_2\right)_t + \left(\int_{\Xi_-}^{\Xi_+} |\mathcal{F}| v_1 \left(E + \frac{h^2}{2F^2}\right) d\xi_2\right)_{\xi_1} & \\ \qquad = \displaystyle\frac{1}{\varepsilon F^2} \int_{\Xi_-}^{\Xi_+} |\mathcal{F}| h \left(-I_0 b_0' v_1 - \varepsilon \mathbf{v}.\boldsymbol{\nabla}_\xi \phi - J_0 \frac{(|\mathcal{F}|^2 v_1^2 + R_l^2 v_2^2)^{3/2}}{(1+c)^2 \, h^p}\right) d\xi_2, & \text{(2.6c)} \end{cases}$$

where we have defined the wetted section S and the average discharge Q by:

$$S = \int_{\Xi_-}^{\Xi_+} \tilde{h} \, d\xi_2 \quad \text{and} \quad Q = \int_{\Xi_-}^{\Xi_+} \tilde{h} v_1 \, d\xi_2.$$

3 Asymptotic expansions

In this section, we expand the fluid velocity field, in the regime $\frac{\varepsilon F^2}{J_0} \ll 1$ and in the quasi-dimensional setting $R_v = R_l \ll 1$. We first consider the transverse equilibrium and show that, asymptotically, the free surface is horizontal. Then, we consider the zeroth-order longitudinal equilibrium where the flow is dominated by the competition between the gravity effects and the bottom friction. Finally, we go a step further in the case where $R_y \ll 1$ to exhibit the first-order asymptotic regime.

3.1 Zeroth-order expansions

In this first part of Section 3, we consider a river with arbitrary meanders, i.e. $R_y = \mathcal{O}(1)$ or $R_y \ll 1$. The goal is to exhibit the zeroth-order asymptotic expansion in $\frac{\varepsilon F^2}{J_0}$ and R_l satisfied by the unknowns of the system.

3.1.1 Transverse equilibrium

In the asymptotic regime under consideration, the equation (2.4) for the free surface elevation reads

$$\frac{\varepsilon}{J_0}(h+\phi)_{\xi_2} = \mathcal{O}\left(\frac{\varepsilon F^2}{J_0} R_y + R_l^2 \left(1 + \frac{\varepsilon F^2}{J_0}\right)\right) = \mathcal{O}\left(\frac{\varepsilon F^2}{J_0} R_y + R_l^2\right).$$

In this framework, there exists a new unknown function $H(\xi_1, t)$ such that

$$\frac{\varepsilon}{J_0}(h(\xi_1,\xi_2,t) + \phi(\xi_1,\xi_2)) = \frac{\varepsilon}{J_0} H(\xi_1, t) + \mathcal{O}(\varepsilon_H), \tag{3.1}$$

where we have set

$$\varepsilon_H = \frac{\varepsilon F^2}{J_0} R_y + R_l^2 \ll 1.$$

3.1.2 Longitudinal equilibrium

Let us now carry out an asymptotic expansion of the fluid velocity field (v_1, v_2). The longitudinal discharge equation (2.3b) can be written as

$$\begin{aligned}\frac{\varepsilon}{J_0}\frac{(h+\phi)_{\xi_1}}{|\mathcal{F}|^2} + \frac{I_0}{J_0}\frac{b_0'}{|\mathcal{F}|^2} + \frac{v_1\sqrt{|\mathcal{F}|^2 v_1^2 + R_l^2 v_2^2}}{(1+c)^2 h^p} \\ = \frac{\varepsilon F^2}{J_0}\left((v_1)_t + v_1(v_1)_{\xi_1} + v_2(v_1)_{\xi_2} + \frac{R_y v_1}{|\mathcal{F}|R(\xi_1)}\left(\frac{\xi_2 R'(\xi_1)}{R(\xi_1)}v_1 - 2v_2\right)\right).\end{aligned} \tag{3.2}$$

For the sake of clarity, we introduce the notation

$$\tilde{\varepsilon} = \frac{\varepsilon F^2}{J_0}(1+R_y) + R_l^2 \ll 1.$$

Recalling the definition (3.1) of the free surface H, the equation (3.2) reads, in the asymptotic regime under consideration, as follows:

$$\frac{1}{|\mathcal{F}|^2}\left(\frac{I_0}{J_0}b_0' + \frac{\varepsilon}{J_0}H_{\xi_1}\right) + \frac{|\mathcal{F}|v_1|v_1|}{(1+c)^2 h^p} = \mathcal{O}(\tilde{\varepsilon}). \tag{3.3}$$

Assuming the asymptotic expansion

$$v_1(\xi_1, \xi_2, t) = v_1^{(0)}(\xi_1, \xi_2, t) + \mathcal{O}(\tilde{\varepsilon})$$

on the longitudinal velocity, the equation (3.3) can be solved, to get

$$|\mathcal{F}|v_1^{(0)}(\xi_1, \xi_2, t) = \frac{\Lambda(\xi_1, \xi_2, t)}{\sqrt{|\Lambda(\xi_1, \xi_2, t)|}}(1 + c(\xi_1, \xi_2))h(\xi_1, \xi_2)^{p/2}, \tag{3.4}$$

where we have defined the corrected slope

$$|\mathcal{F}(\xi_1, \xi_2)|\Lambda(\xi_1, \xi_2, t) = \left(-\frac{I_0}{J_0}b_0'(\xi_1) - \frac{\varepsilon}{J_0}H_{\xi_1}(\xi_1, t)\right). \tag{3.5}$$

From this expansion, we can deduce an expansion of the transverse velocity v_2 by assuming that $v_2 = v_2^{(0)} + \mathcal{O}(\tilde{\varepsilon})$ and using the mass conservation law:

$$\left(\tilde{h}v_2^{(0)}\right)_{\xi_2} = -\tilde{h}_t - \left(\tilde{h}v_1^{(0)}\right)_{\xi_1} + \mathcal{O}(\tilde{\varepsilon}).$$

Then, we get

$$\tilde{h}v_2^{(0)}(\xi_1, \xi_2, t) = -\int_{\Xi_-(\xi_1,t)}^{\xi_2}\left(\tilde{h}_t - \left(\tilde{h}v_1^{(0)}\right)_{\xi_1}\right)(\xi_1, \eta, t)d\eta + \mathcal{O}(\tilde{\varepsilon}).$$

Finally, note that the width-integrated longitudinal discharge Q also satisfies $Q = Q^{(0)} + \mathcal{O}(\tilde{\varepsilon})$. Arguing the definition (3.4) of $v_1^{(0)}$, we get the following expansion:

$$Q^{(0)} := \int_{\Xi_-}^{\Xi_+}\tilde{h}v_1^{(0)}\,d\xi_2 = \int_{\Xi_-}^{\Xi_+}\sqrt{|\Lambda|}\,\mathrm{sgn}(\Lambda)(1+c)h^{1+p/2}\,d\xi_2.$$

Noting that $(|\mathcal{F}|\Lambda)_{\xi_2} = 0$ and that $\mathrm{sgn}(\Lambda)$ does not depend on ξ_2 since the dependency in ξ_2 of Λ comes from $|\mathcal{F}| > 0$, the definition of $Q^{(0)}$ can be simplified as follows:

$$Q^{(0)} = \sqrt{|\mathcal{F}||\Lambda|}\,\mathrm{sgn}(\Lambda)\int_{\Xi_-}^{\Xi_+}\frac{(1+c)h^{1+p/2}}{\sqrt{|\mathcal{F}|}}\,d\xi_2. \tag{3.6}$$

3.2 First-order expansion

So far, we have provided a zeroth-order expansion of the unknowns of the problem, with respect to ε_H and $\tilde{\varepsilon}$. Let us now consider the next order. If we consider the general case $R_y = \mathcal{O}(1)$, going further to a first-order expansion would be troublesome since, in this case, $\varepsilon_H = \mathcal{O}(\frac{\varepsilon F^2}{J_0})$. As a result, we would get a term in $\frac{\varepsilon F^2}{J_0} R_y$ in the first-order expansion of H, which would make all computations barely tractable.

Therefore, for $R_y = \mathcal{O}(1)$, we will only consider the previously determined zeroth-order expansion from now on. If $R_y \ll 1$ (i.e. for a weakly meandering river), and if we assume $R_l = \mathcal{O}(\frac{\varepsilon F^2}{J_0})$ as well as $R_y = \mathcal{O}(\frac{\varepsilon F^2}{J_0})$, we get $\varepsilon_H = \mathcal{O}((\frac{\varepsilon F^2}{J_0})^2)$ and $\tilde{\varepsilon} = \mathcal{O}((\frac{\varepsilon F^2}{J_0})^2)$. In this context, we are able to write a tractable first-order expansion of the longitudinal fluid velocity.

By rewriting the equation (3.2) and by taking into account these asymptotic expansions, we get:

$$\frac{|\mathcal{F}|(v_1^{(0)}|v_1^{(0)}| - v_1|v_1|)}{(1+c)^2 h^p} = \frac{\varepsilon F^2}{J_0}\Big((v_1)_t + v_1(v_1)_{\xi_1} + v_2(v_1)_{\xi_2}\Big) + \mathcal{O}\left(\left(\frac{\varepsilon F^2}{J_0}\right)^2\right).$$

Therefore, if $v_1 = v_1^{(0)} + \frac{\varepsilon F^2}{J_0} v_1^{(1)} + \mathcal{O}((\frac{\varepsilon F^2}{J_0})^2)$, we immediately obtain:

$$v_1^{(1)} = -\frac{|\mathcal{F}| v_1^{(0)}}{2\Lambda}\left(\left(v_1^{(0)}\right)_t + v_1^{(0)}\left(v_1^{(0)}\right)_{\xi_1} + v_2^{(0)}\left(v_1^{(0)}\right)_{\xi_2}\right). \tag{3.7}$$

Equipped with the above formula for $v_1^{(1)}$, we are now in a position to compute the first-order expansion of Q, defined by $Q^{(1)} = \int_{\Xi_-}^{\Xi_+} \tilde{h} v_1^{(1)}\, d\xi_2$. Using the chain rule, arguing the mass conservation equation and performing straightforward computations, we get

$$Q^{(1)} = -\int_{\Xi_-}^{\Xi_+} \frac{|\mathcal{F}|}{4\Lambda}\left(\tilde{h}\left(v_1^{(0)}\right)^2\right)_t d\xi_2 - \int_{\Xi_-}^{\Xi_+} \frac{|\mathcal{F}|}{4\Lambda}\left(\tilde{h}\left(v_1^{(0)}\right)^3\right)_{\xi_1} d\xi_2.$$

Remark that $|\mathcal{F}| = 1 + \mathcal{O}(\frac{\varepsilon F^2}{J_0})$. Therefore, the following expression of $Q^{(1)}$ is equivalent to the above formula, up to $\mathcal{O}(\frac{\varepsilon F^2}{J_0})$:

$$Q^{(1)} = \frac{-1}{4|\mathcal{F}|\Lambda}\left[\left(\int_{\Xi_-}^{\Xi_+} \tilde{h} v_1^2\, d\xi_2\right)_t + \left(\int_{\Xi_-}^{\Xi_+} \tilde{h} v_1^3\, d\xi_2\right)_{\xi_1}\right]. \tag{3.8}$$

4 Zeroth-order two-equation model for a strongly meandering river

In this Section, we assume that the river is strongly meandering, meaning that $R_y = \mathcal{O}(1)$, and we derive a 1D section-averaged model which is consistent up to $O(\frac{\varepsilon F^2}{J_0})$ with the 2D shallow water system. The variables of this new model should only depend on t and ξ_1, although an underlying 2D dependency will remain for known quantities (e.g. the shape of the channel or the friction distribution).

We start with the section-averaged mass and x-discharge equations (2.6a) – (2.6b). The mass conservation equation is already written in a 1D form, with the 1D variables S and Q, and there is nothing further to do. To get a zeroth-order model, the discharge equation of the 1D model must be consistent with (2.6b) up to $\mathcal{O}(1)$, since (2.6b) contains $\frac{J_0}{\varepsilon F^2}$. In this context, the equation (2.6b) rewrites as follows, since $(|\mathcal{F}|\Lambda)_{\xi_2} = 0$:

$$Q_t + \left(\int_{\Xi_-}^{\Xi_+} \tilde{h} v_1^2\, d\xi_2\right)_{\xi_1} = \frac{J_0}{\varepsilon F^2}\left(|\mathcal{F}|\Lambda \int_{\Xi_-}^{\Xi_+} \frac{\tilde{h}}{|\mathcal{F}|^2}\, d\xi_2 - \int_{\Xi_-}^{\Xi_+} \frac{|\mathcal{F}| v_1 |v_1|}{(1+c)^2 h^{p-1}}\, d\xi_2\right) + \mathcal{O}(1). \tag{4.1}$$

The higher-order terms of the above equation lie in its right-hand side. Therefore, the first step to writing a model with 1D variables is to derive a friction model, similar to the usual engineering ones and consistent up to $\mathcal{O}(\frac{\varepsilon F^2}{J_0})$.

We thus seek $(C_h)_m$ such that

$$\int_{\Xi_-}^{\Xi_+} \frac{|\mathcal{F}|v_1|v_1|}{(1+c)^2 h^{p-1}}\, d\xi_2 = S_m \frac{Q|Q|}{(C_h)_m^2 R_h S^2} + \mathcal{O}\left(\frac{\varepsilon F^2}{J_0}\right) =: S_m \mathcal{J}_m + \mathcal{O}\left(\frac{\varepsilon F^2}{J_0}\right),$$

where S_m is defined by

$$S_m := \int_{\Xi_-}^{\Xi_+} \frac{\tilde{h}}{|\mathcal{F}|^2}\, d\xi_2.$$

To recover the required equilibrium between the corrected slope $|\mathcal{F}|\Lambda$ and the friction model $\mathcal{J}_m$, the expression of $(C_h)_m$ has to ensure that $|\mathcal{F}|\Lambda - \mathcal{J}_m = \mathcal{O}(\frac{\varepsilon F^2}{J_0})$. In addition, we wish to make sure that the model under consideration correctly recovers the zeroth-order expansion $Q = Q^{(0)} + \mathcal{O}(\frac{\varepsilon F^2}{J_0})$, where $Q^{(0)}$ is given by (3.6). For both these statements to hold, it is sufficient to choose $(C_h)_m$ such that $|\mathcal{F}|\Lambda = \frac{Q^{(0)}|Q^{(0)}|}{(C_h)_m^2 R_h S^2}$, that is to say

$$(C_h)_m^2 R_h = \frac{Q^{(0)}|Q^{(0)}|}{|\mathcal{F}|\Lambda S^2}.$$

Let us note that, although $(C_h)_m$ contains Λ, it does not contain a differential term since $Q^{(0)}$ also contains Λ. This remark also applies to $\mathcal{J}_m$. The discharge equation (4.1) then rewrites:

$$Q_t + \left(\int_{\Xi_-}^{\Xi_+} \tilde{h} v_1^2\, d\xi_2\right)_{\xi_1} = \frac{J_0}{\varepsilon F^2} S(|\mathcal{F}|\Lambda - \mathcal{J}_m) + \mathcal{O}(1). \tag{4.2}$$

The second and last step to obtain the 1D discharge equation is to rewrite it under the classical form of a balance law. Introducing the longitudinal slope $\mathcal{I}$ as

$$\mathcal{I} = -\frac{I_0}{J_0} b_0',$$

we note that $|\mathcal{F}|\Lambda = \mathcal{I} - \frac{\varepsilon}{J_0} H_{\xi_1}$, and we are thus able to regroup the differential terms in the left-hand side of (4.2). Finally, by analogy with the classical shallow water system in (S, Q) variables, let us approximate $\int_{\Xi_-}^{\Xi_+} \tilde{h} v_1^2\, d\xi_2$ with $\frac{Q^2}{S}$, which is valid up to $\mathcal{O}(1)$. The complete zeroth-order 1D model for a meandering river thus reads:

$$\begin{cases} S_t + Q_x = 0 \\ Q_t + \left(\dfrac{Q^2}{S}\right)_{\xi_1} + \dfrac{S H_{\xi_1}}{F^2} = \dfrac{J_0}{\varepsilon F^2} S(\mathcal{I} - \mathcal{J}_m), \end{cases}$$

where the friction model $\mathcal{J}_m$ satisfies, using the expression (3.6) of $Q^{(0)}$, the following chain of equalities:

$$\mathcal{J}_m = \frac{Q|Q|}{(C_h)_m^2 R_h S^2} = |\mathcal{F}|\Lambda \frac{Q|Q|}{Q^{(0)}|Q^{(0)}|} = Q|Q| \left(\int_{\Xi_-}^{\Xi_+} \frac{(1+c) h^{1+p/2}}{\sqrt{|\mathcal{F}|}}\, d\xi_2\right)^{-2}.$$

As a consequence, we readily note that $\mathcal{J}_m$ does not contain any differential term, since it does not depend on Λ.

This is the canonical form of section-averaged shallow water equations found in the literature: see [Decoene et al., 2009] and references therein. We removed $\mathcal{O}(1)$ terms accounting for the influence of the meandering in order to get a simple formulation of the shallow water model. However, the form of the source term ensures the consistency of this shallow water model up to order $\mathcal{O}(\frac{\varepsilon F^2}{J_0})$ with the 2D shallow water equations, which is far from being obvious for other similar models. By construction, our model conserves the fluid mass and is consistent up to $\mathcal{O}(\frac{\varepsilon F^2}{J_0})$ with the 2D model in the asymptotic regime under consideration. In addition, its homogeneous form is hyperbolic, by analogy with the classical shallow water model in (S, Q) variables.

5 First-order four-equation model for a weakly meandering river

We now assume that the river is weakly meandering, meaning that $R_y = \mathcal{O}(\frac{\varepsilon F^2}{J_0}) \ll 1$. The goal of this section is to derive a suitable 1D model, consistent up to first-order (i.e. up to $\mathcal{O}((\frac{\varepsilon F^2}{J_0})^2)$) with the 2D system (2.3) – (2.5). Similarly to the strongly meandering case, the variables of this new model should only depend on t and ξ_1.

To that end, we start with the section-averaged system (2.6), and we introduce a relevant friction model as well as new 1D variables. Then, we propose an Euler-like four-equation model to satisfy the asymptotic regime under consideration. Finally, we exhibit some mathematical properties satisfied by this new system.

5.1 Consistent section-averaged system

To consider a first-order model, we set the forthcoming developments in the context of Section 3.2, i.e. we assume that $R_l = \mathcal{O}(\frac{\varepsilon F^2}{J_0})$ and $R_y = \mathcal{O}(\frac{\varepsilon F^2}{J_0})$. In this case, we have $|\mathcal{F}| = 1 + \mathcal{O}(R_y) = 1 + \mathcal{O}(\frac{\varepsilon F^2}{J_0})$, and thus $\tilde{h} = h + \mathcal{O}(\frac{\varepsilon F^2}{J_0})$. These remarks allow us to write the following asymptotic expansion of the integrated system (2.6):

$$\begin{cases} S_t + Q_{\xi_1} = 0, & \text{(5.1a)} \\ Q_t + \left(\displaystyle\int_{\Xi_-}^{\Xi_+} \tilde{h} v_1^2 \, d\xi_2 \right)_{\xi_1} = \frac{J_0}{\varepsilon F^2} \left(|\mathcal{F}| \Lambda \displaystyle\int_{\Xi_-}^{\Xi_+} \frac{\tilde{h}}{|\mathcal{F}|^2} \, d\xi_2 - \int_{\Xi_-}^{\Xi_+} \frac{\tilde{h} |\mathcal{F}| v_1 |v_1|}{(1+c)^2 h^p} \, d\xi_2 \right) + \mathcal{O}\left(\frac{\varepsilon F^2}{J_0} \right), & \text{(5.1b)} \\ \left(\displaystyle\int_{\Xi_-}^{\Xi_+} \frac{1}{2} \tilde{h} v_1^2 \, d\xi_2 \right)_t + \left(\displaystyle\int_{\Xi_-}^{\Xi_+} \frac{1}{2} \tilde{h} v_1^3 \, d\xi_2 \right)_{\xi_1} = \frac{J_0}{\varepsilon F^2} \left(|\mathcal{F}| \Lambda Q - \displaystyle\int_{\Xi_-}^{\Xi_+} \frac{\tilde{h} v_1 |\mathcal{F}|^3 v_1 |v_1|}{(1+c)^2 h^p} \, d\xi_2 \right) + \mathcal{O}\left(\frac{\varepsilon F^2}{J_0} \right). & \text{(5.1c)} \end{cases}$$

The goal of the remainder of this section is to propose a 1D model that is first-order accurate with respect to the small parameter $\frac{\varepsilon F^2}{J_0}$. That is to say, contrary to section 4 where we had the zeroth-order expansion $Q = Q^{(0)} + \mathcal{O}(\frac{\varepsilon F^2}{J_0})$, we now wish to recover a higher accuracy: $Q = Q^{(0)} + \frac{\varepsilon F^2}{J_0} Q^{(1)} + \mathcal{O}((\frac{\varepsilon F^2}{J_0})^2)$.

In order to address this issue, we first consider a zeroth-order approximation of the discharge equation, like in section 4. This approximation is obtained by defining a relevant friction model. Equipped with this friction model, we turn to providing a consistent approximation of the energy equation up to first-order in $\frac{\varepsilon F^2}{J_0}$. Finally, we propose a conservative form of the proposed first-order system.

5.1.1 The friction model

In order to get a 1D system from the integrated equations (5.1), we introduce a model for the friction term, consistent with the standard engineering ones. Starting with the discharge equation (5.1b), we seek a 1D friction model that is consistent with the 2D friction term up to $\mathcal{O}(\frac{\varepsilon F^2}{J_0})$. Note that this $\mathcal{O}(\frac{\varepsilon F^2}{J_0})$ error on the friction term translates to a $\mathcal{O}(1)$ error on the whole discharge equation. Thanks to this remark, we instead choose to approximate the friction term of the energy equation

$$\int_{\Xi_-}^{\Xi_+} \frac{\tilde{h} |\mathcal{F}|^3 v_1 |v_1|}{(1+c)^2 h^p} \, d\xi_2 = \int_{\Xi_-}^{\Xi_+} \frac{\tilde{h} |\mathcal{F}| v_1 |v_1|}{(1+c)^2 h^p} \, d\xi_2 + \mathcal{O}(R_y).$$

This algebraic manipulation is possible since it only introduces an error in $\mathcal{O}(R_y) = \mathcal{O}(\frac{\varepsilon F^2}{J_0})$. The advantage of this approach is to stay consistent with the friction term of the energy equation, which contains $|\mathcal{F}|^3$ instead of $|\mathcal{F}|$, and where we will not be able to introduce an $\mathcal{O}(\frac{\varepsilon F^2}{J_0})$ error.

We now proceed in a similar way as in Section 4. Noting that a zeroth-order expansion of the integrated discharge equation (5.1b) reads as follows:

$$Q_t + \left(\int_{\Xi_-}^{\Xi_+} \tilde{h} v_1^2 \, d\xi_2 \right)_{\xi_1} = \frac{J_0}{\varepsilon F^2} \left(|\mathcal{F}| \Lambda S - \int_{\Xi_-}^{\Xi_+} \frac{\tilde{h} |\mathcal{F}|^3 v_1 |v_1|}{(1+c)^2 h^p} \, d\xi_2 \right) + \mathcal{O}(1),$$

we therefore seek C_h such that

$$\int_{\Xi_-}^{\Xi_+} \frac{\tilde{h} |\mathcal{F}|^3 v_1 |v_1|}{(1+c)^2 h^p} \, d\xi_2 = S \frac{Q|Q|}{C_h^2 R_h S^2} + \mathcal{O}\left(\frac{\varepsilon F^2}{J_0} \right) =: S\mathcal{J} + \mathcal{O}\left(\frac{\varepsilon F^2}{J_0} \right).$$

Like in Section 4, it is sufficient to choose C_h such that $|\mathcal{F}|\Lambda = \frac{Q^{(0)}|Q^{(0)}|}{C_h^2 R_h S^2}$, that is to say

$$C_h^2 R_h = \frac{Q^{(0)}|Q^{(0)}|}{|\mathcal{F}|\Lambda S^2}. \tag{5.2}$$

We then rewrite the discharge equation (2.6b) as follows:

$$Q_t + \left(\int_{\Xi_-}^{\Xi_+} h v_1^2 \, d\xi_2 \right)_{\xi_1} = \frac{J_0}{\varepsilon F^2} S(|\mathcal{F}|\Lambda - \mathcal{J}) + \mathcal{O}(1). \tag{5.3}$$

The term $|\mathcal{F}|\Lambda$ of this equation contains the differential term H_{ξ_1}, which should be included in the flux rather than in the source term. This discrepancy will be dealt with in a later Section.

Let us note that $\mathcal{J}$ does not contain any differential term coming from Λ, even though Λ contains H_{ξ_1}. Indeed, since $Q^{(0)}$ is given by (3.6) and C_h is given by (5.2), we have the following sequence of equalities:

$$\mathcal{J} = \frac{Q|Q|}{C_h^2 R_h S^2} = |\mathcal{F}|\Lambda \frac{Q|Q|}{Q^{(0)}|Q^{(0)}|} = Q|Q| \left(\int_{\Xi_-}^{\Xi_+} \frac{(1+c) h^{1+p/2}}{\sqrt{|\mathcal{F}|}} \, d\xi_2 \right)^{-2}. \tag{5.4}$$

5.1.2 Consistent energy equation

The discharge equation (5.3), thanks to the friction model (5.2), correctly recovers the zeroth-order asymptotic expansion $Q = Q^{(0)} + \mathcal{O}(\frac{\varepsilon F^2}{J_0})$ when $\frac{\varepsilon F^2}{J_0} \to 0$. As a consequence, plugging this friction model into the classical shallow water system would be sufficient to ensure the accuracy of this asymptotic expansion. However, we wish to go one step further and actually get accuracy up to the first-order asymptotic expansion

$$Q = Q^{(0)} + \frac{\varepsilon F^2}{J_0} Q^{(1)} + \mathcal{O}\left(\left(\frac{\varepsilon F^2}{J_0} \right)^2 \right),$$

where $Q^{(1)}$ is given by (3.8). This accurate first-order expansion will be achieved by deriving a suitable approximation of the integrated energy equation (2.6c). Such an approach was already suggested to derive consistent shallow water models for thin film flows down an incline [Luchini and Charru, 2010].

In order to mimic the structure of Euler equations for numerical simulation purpose and ensure a good mathematical structure, we search for an averaged energy equation that could be derived from the momentum equation. Thus, we search for a source term in the energy equation that is the product of the source term in the momentum equation with the discharge rate. The source term of this new energy balance law, plugging the asymptotic expansion (3.6) – (3.8) into the expression (5.4) of the friction model $\mathcal{J}$, satisfies:

$$\frac{J_0}{\varepsilon F^2} Q(|\mathcal{F}|\Lambda - \mathcal{J}) = -2|\mathcal{F}|\Lambda Q^{(1)} + \mathcal{O}\left(\frac{\varepsilon F^2}{J_0} \right).$$

Since $Q^{(1)}$ is given by (3.8), the new energy equation reads

$$\left(\frac{1}{2}\int_{\Xi_-}^{\Xi_+}\tilde{h}v_1^2\,d\xi_2\right)_t+\left(\frac{1}{2}\int_{\Xi_-}^{\Xi_+}\tilde{h}v_1^3\,d\xi_2\right)_{\xi_1}=\frac{J_0}{\varepsilon F^2}Q(|\mathcal{F}|\Lambda-\mathcal{J}). \tag{5.5}$$

This energy equation is consistent with the averaged energy equation (5.1c) up to $\mathcal{O}(\frac{\varepsilon F^2}{J_0})$.

5.1.3 Final conservative form of the integrated 2D system

Thanks to the friction model (5.2) and therefore the equations (5.3) and (5.5), the system (5.1) rewrites:

$$\begin{cases} S_t+Q_{\xi_1}=0,\\ Q_t+\left(\displaystyle\int_{\Xi_-}^{\Xi_+}\tilde{h}v_1^2\,d\xi_2\right)_{\xi_1}=\frac{J_0}{\varepsilon F^2}S(|\mathcal{F}|\Lambda-\mathcal{J})+\mathcal{O}(1),\\ \left(\displaystyle\frac{1}{2}\int_{\Xi_-}^{\Xi_+}\tilde{h}v_1^2\,d\xi_2\right)_t+\left(\frac{1}{2}\int_{\Xi_-}^{\Xi_+}\tilde{h}v_1^3\,d\xi_2\right)_{\xi_1}=\frac{J_0}{\varepsilon F^2}Q(|\mathcal{F}|\Lambda-\mathcal{J})+\mathcal{O}\left(\frac{\varepsilon F^2}{J_0}\right). \end{cases} \tag{5.6}$$

This system is consistent with the integrated 2D equations (5.1). In addition, by construction, this system ensures the accuracy of the asymptotic expansion $Q=Q^{(0)}+\frac{\varepsilon F^2}{J_0}Q^{(1)}+\mathcal{O}((\frac{\varepsilon F^2}{J_0})^2)$ when $\frac{\varepsilon F^2}{J_0}\to 0$.

Note that Λ contains the space derivative H_{ξ_1}. No differential term should remain in the source; rather, they should be regrouped in the flux to get a good mathematical structure. Since $|\mathcal{F}|\Lambda$ is given by (3.5), the system (5.6) is equivalent to

$$\begin{cases} S_t+Q_{\xi_1}=0,\\ Q_t+\left(\displaystyle\int_{\Xi_-}^{\Xi_+}\tilde{h}v_1^2\,d\xi_2\right)_{\xi_1}+\frac{SH_{\xi_1}}{F^2}=\frac{J_0}{\varepsilon F^2}S(\mathcal{I}-\mathcal{J})+\mathcal{O}(1),\\ \left(\displaystyle\frac{1}{2}\int_{\Xi_-}^{\Xi_+}\tilde{h}v_1^2\,d\xi_2\right)_t+\left(\frac{1}{2}\int_{\Xi_-}^{\Xi_+}\tilde{h}v_1^3\,d\xi_2\right)_{\xi_1}+\frac{QH_{\xi_1}}{F^2}=\frac{J_0}{\varepsilon F^2}Q(\mathcal{I}-\mathcal{J})+\mathcal{O}\left(\frac{\varepsilon F^2}{J_0}\right). \end{cases} \tag{5.7}$$

The above system can be recast under a conservative form. Let us define $L(\xi_1,z)$ such that $S=\int_0^H L(z)\,dz$, see Figure 2. First, note the following chain of equalities:

$$\frac{SH_{\xi_1}}{F^2}=\frac{H_{\xi_1}}{F^2}\int_0^H L\,dz=\left(\frac{1}{F^2}\int_0^H(H-z)L\,dz\right)_{\xi_1}-\frac{1}{F^2}\int_0^H(H-z)L_{\xi_1}\,dz=:P^{hy}_{\xi_1}-P^{lat},$$

where P^{hy} is the hydrostatic pressure and P^{lat} is the lateral pressure. In addition, remark that

$$\frac{QH_{\xi_1}}{F^2}=\frac{HS_t+(HQ)_{\xi_1}}{F^2}=\left(\frac{1}{F^2}\int_0^H zL\,dz\right)_t+\left(\frac{U}{F^2}\left(\int_0^H HL\,dz\right)\right)_{\xi_1}=:\mathcal{E}_t+(U(\mathcal{E}+P^{hy}))_{\xi_1},$$

where $\mathcal{E}$ is the potential gravity energy, and where the averaged flow velocity U is defined by $U=Q/S$.

Therefore, the system (5.7) reads:

$$\begin{cases} S_t + Q_{\xi_1} = 0, & \text{(5.8a)} \\ Q_t + \left(P^{hy} + \displaystyle\int_{\Xi_-}^{\Xi_+} \tilde{h} v_1^2 \, d\xi_2 \right)_{\xi_1} = P^{lat} + \frac{J_0}{\varepsilon F^2} S(\mathcal{I} - \mathcal{J}) + \mathcal{O}(1), & \text{(5.8b)} \\ \left(\mathcal{E} + \frac{1}{2} \displaystyle\int_{\Xi_-}^{\Xi_+} \tilde{h} v_1^2 \, d\xi_2 \right)_t + \left(\mathcal{E} + P^{hy} + \frac{1}{2} \displaystyle\int_{\Xi_-}^{\Xi_+} \tilde{h} v_1^3 \, d\xi_2 \right)_{\xi_1} = \frac{J_0}{\varepsilon F^2} Q(\mathcal{I} - \mathcal{J}) + \mathcal{O}\left(\frac{\varepsilon F^2}{J_0} \right). & \text{(5.8c)} \end{cases}$$

The above equations are written under the form of a system of balance laws, where no differential terms subsist in the source term. They are consistent with the width-integrated equations (5.1) and they ensure the first-order asymptotic expansion of the discharge $Q = Q^{(0)} + \frac{\varepsilon F^2}{J_0} Q^{(1)} + \mathcal{O}((\frac{\varepsilon F^2}{J_0})^2)$ when $\frac{\varepsilon F^2}{J_0} \to 0$.

5.2 An Euler-like model

We now wish to recast the above 1D system under an Euler-like formulation to eliminate the integral terms and to ensure relevant mathematical properties, such as hyperbolicity. We first introduce a relevant energy and pressure. Then, we add a fourth equation to the model to account for the temporal variations of the pressure. We briefly recall the classical form of the 1D homogeneous Euler system:

$$\begin{cases} S_t + (SU)_{\xi_1} = 0, \\ (SU)_t + \left(SU^2 + P \right)_{\xi_1} = 0, \\ E_t + (U(E+P))_{\xi_1} = 0, \end{cases}$$

where $U = Q/S$ is the velocity, E is the energy and P is the pressure, usually given by a pressure law $P(S, U, E)$. A well-known example of a pressure law is the ideal gas law, defined by $P = (\gamma - 1)(E - SU^2/2)$, with $\gamma \geq 1$.

5.2.1 Introduction of an energy and a pressure

The mass conservation equation (5.8a) is exact and similar to that of the Euler system, so no work needs to be done on this equation. Next, consider the discharge balance equation (5.8b). To recover an Euler-like formulation, we introduce a pressure P such that

$$\int_{\Xi_-}^{\Xi_+} \tilde{h} v_1^2 \, d\xi_2 + P^{hy} = SU^2 + P. \tag{5.9}$$

As a consequence, it is natural to introduce a new variable Ψ, the so-called enstrophy [Richard and Gavrilyuk, 2012], defined by

$$\int_{\Xi_-}^{\Xi_+} \tilde{h} v_1^2 \, d\xi_2 = SU^2 + S^3 \Psi. \tag{5.10}$$

The pressure P defined by (5.9) becomes

$$P = P^{hy} + S^3 \Psi. \tag{5.11}$$

By inspection of the time derivative within the energy balance equation (5.8c), we propose the following natural definition of the energy:

$$E = \mathcal{E} + \frac{1}{2} SU^2 + \frac{1}{2} S^3 \Psi,$$

such that the time derivative is applied to E. To take care of the spatial derivative in this equation, we introduce the variable Π, taking inspiration from the definition (5.10) of Ψ:

$$\int_{\Xi_-}^{\Xi_+} \tilde{h} v_1^3 \, d\xi_2 = U \left(SU^2 + S^3 \Pi \right).$$

In order to better understand the roles played by the new variables Ψ and Π, let us rewrite each of them as a single integral. Straightforward computations yield the following expressions:

$$S^3\Psi = \int_{\Xi_-}^{\Xi_+} \tilde{h}(v_1 - U)^2 \, d\xi_2 \qquad \text{and} \qquad S^3\Pi = \int_{\Xi_-}^{\Xi_+} \tilde{h}(v_1 - U)^2 \Big(2 + \frac{v_1}{U}\Big) \, d\xi_2.$$

The variable $S^3\Psi$ accounts for the vorticity of the flow in the cross-stream direction: it is the variance of the fluid velocity u in the cross-stream direction. The variable $S^3\Pi$ plays the role of and will be referred to as a potential. According to these definitions, we suggest the following fully 1D model to replace the averaged 2D system (5.8):

$$\begin{cases} S_t + Q_{\xi_1} = 0, \\ Q_t + \left(\dfrac{Q^2}{S} + P\right)_{\xi_1} = P^{lat} + \dfrac{J_0}{\varepsilon F^2} S(\mathcal{I} - \mathcal{J}), \\ E_t + \left(\dfrac{Q}{S}(E+P)\right)_{\xi_1} + \left(\dfrac{1}{2}\dfrac{Q}{S} S^3(\Pi - 3\Psi)\right)_{\xi_1} = \dfrac{J_0}{\varepsilon F^2} Q(\mathcal{I} - \mathcal{J}). \end{cases} \tag{5.12}$$

5.2.2 A four-equation Euler-like model

The time evolution of the potential $S^3\Pi$ is not prescribed by the three-equation system (5.12). Therefore, we need to add an equation to this system, whose time derivative will have to contain $S^3\Pi$. In addition, compared to a classical Euler system, the energy equation of (5.12) has an extra differential term. These remarks prompt us to introduce a new arbitrary variable $e = e(S, \Psi, \Pi)$, corresponding to an internal energy, and governed by the following equation:

$$e_t + \left(\frac{Q}{S}\left(e - \frac{1}{2} S^3(\Pi - 3\Psi)\right)\right)_{\xi_1} = 0.$$

Adding this equation to the system (5.12) yields the following four-equation model:

$$\begin{cases} S_t + Q_{\xi_1} = 0, \\ Q_t + \left(\dfrac{Q^2}{S} + P\right)_{\xi_1} = P^{lat} + \dfrac{J_0}{\varepsilon F^2} S(\mathcal{I} - \mathcal{J}), \\ (E+e)_t + \left(\dfrac{Q}{S}(E + e + P)\right)_{\xi_1} = \dfrac{J_0}{\varepsilon F^2} Q(\mathcal{I} - \mathcal{J}), \\ e_t + \left(\dfrac{Q}{S}\left(e - \dfrac{1}{2} S^3(\Pi - 3\Psi)\right)\right)_{\xi_1} = 0. \end{cases} \tag{5.13}$$

The homogeneous part of the first three equations of this model correspond to an Euler model with energy $E+e$.

The four-equation model (5.13) is consistent with the width-integrated 2D shallow water equations (5.1) whatever the choice of the internal energy e. However, its hyperbolicity will depend on the choice of e: let us then determine $e = e(S, \Psi, \Pi)$ such that the above four-equation system is hyperbolic. We consider

$$e = \frac{1}{2} S^3(\alpha\Psi + \beta\Pi), \text{ with } \alpha \in \mathbb{R} \text{ and } \beta \in \mathbb{R}^*,$$

to mimic the form of the term $\frac{1}{2} S^3(\Pi - 3\Psi)$ that needs to be canceled. Straightforward computations show that the choice $\alpha = -3$ and $\beta = 1$ yields a hyperbolic system with the stationary wave $e_t = 0$ and whose characteristic velocities (i.e. the eigenvalues of the Jacobian matrix of the flux function) are given by:

$$0, \; U, \; U \pm \sqrt{\frac{S}{F^2 L(H)} + S^2\Pi}.$$

As a consequence of the choice $\alpha = -3$ and $\beta = 1$, the four-equation model (5.13) reads, in variables (S, Q, E, e):

$$\begin{cases} S_t + Q_{\xi_1} = 0, \\ Q_t + \left(\dfrac{Q^2}{S} + P\right)_{\xi_1} = P^{lat} + \dfrac{J_0}{\varepsilon F^2} S(\mathcal{I} - \mathcal{J}), \\ (E+e)_t + \left(\dfrac{Q}{S}(E + e + P)\right)_{\xi_1} = \dfrac{J_0}{\varepsilon F^2} Q(\mathcal{I} - \mathcal{J}), \\ e_t = 0. \end{cases} \tag{5.14}$$

The structure of the homogeneous part of this system mimics that of the classical Euler system with an additional stationary wave. In this context, the pressure law is

$$P(S, U, E) = 2E - SU^2 + P^{hy} - 2\mathcal{E} = 2\left(E - \frac{1}{2}SU^2\right) + \frac{1}{F^2}\int_0^H (H - 3z) L dz.$$

Remark that the non-geometrical terms of this pressure law are similar to the usual ideal gas law of the Euler system of gas dynamics. Also, note that the total energy $E + e$ has a physical meaning. Indeed, we have

$$\begin{aligned} E + e &= \frac{1}{2}\frac{Q^2}{S} + \frac{1}{2}S^3(\Pi - 2\Psi) + \mathcal{E} \\ &= \mathcal{E} + \frac{1}{2}SU^2 + \frac{1}{2}\int_{\Xi_-}^{\Xi_+} \tilde{h}(v_1 - U)^2 \, d\xi_2 + \frac{1}{2U}\int_{\Xi_-}^{\Xi_+} \tilde{h}(v_1 - U)^3 \, d\xi_2. \end{aligned}$$

Therefore, the total energy corresponds to the sum of the potential energy, the kinetic energy, and the quadratic and cubic errors with respect to the averaged velocity U.

For future reference, let us also write the system (5.14) in the set of variables (S, Q, Ψ, Π):

$$\begin{cases} S_t + Q_{\xi_1} = 0, \\ Q_t + \left(\dfrac{Q^2}{S} + S^3\Psi\right)_{\xi_1} + \dfrac{SH_{\xi_1}}{F^2} = \dfrac{J_0}{\varepsilon F^2} S(\mathcal{I} - \mathcal{J}), \\ \left(\dfrac{1}{2}\dfrac{Q^2}{S} + \dfrac{1}{2}S^3\Psi\right)_t + \left(\dfrac{Q}{S}\left(\dfrac{1}{2}\dfrac{Q^2}{S} + \dfrac{1}{2}S^3\Pi\right)\right)_{\xi_1} + \dfrac{QH_{\xi_1}}{F^2} = \dfrac{J_0}{\varepsilon F^2} Q(\mathcal{I} - \mathcal{J}), \\ \left(\dfrac{1}{2}S^3(\Pi - 3\Psi)\right)_t = 0. \end{cases} \tag{5.15}$$

5.2.3 Consistency of the new model with the asymptotic expansions

At this level, the zeroth-order asymptotic expansion of the discharge Q is satisfied by construction of the discharge equation, see Section 5.1. However, we also wish to recover its first-order asymptotic expansion, from which the energy equation of the model (5.15) is based. To that end, we necessarily need to ensure the zeroth-order asymptotic expansions of Ψ and Π for the left-hand side of the energy equation to be consistent with the asymptotic regime. Therefore, the following asymptotic expansions on the discharge, enstrophy and potential have to be satisfied by the final four-equation model:

$$Q = Q^{(0)} + \frac{\varepsilon F^2}{J_0} Q^{(1)} + \mathcal{O}\left(\left(\frac{\varepsilon F^2}{J_0}\right)^2\right), \quad \Psi = \Psi^{(0)} + \mathcal{O}\left(\frac{\varepsilon F^2}{J_0}\right) \quad \text{and} \quad \Pi = \Pi^{(0)} + \mathcal{O}\left(\frac{\varepsilon F^2}{J_0}\right). \tag{5.16}$$

To write the expressions of $\Psi^{(0)}$ and $\Pi^{(0)}$ in a more compact way, we introduce the following simplified notation:

$$\mathcal{M}_n = \int_{\Xi_-}^{\Xi_+} \tilde{h}\left(\frac{(1+c)\, h^{p/2}}{|\mathcal{F}|^{3/2}}\right)^n d\xi_2.$$

Using this notation, we immediately obtain $S = \mathcal{M}_0$ and $Q^{(0)} = \sqrt{|\mathcal{F}||\Lambda|}\,\mathrm{sgn}(\Lambda)\,\mathcal{M}_1$. In addition, straightforward computations yield the following asymptotic expansions for Ψ and Π:

$$S^3\Psi^{(0)} = |\mathcal{F}||\Lambda|\left(\mathcal{M}_2 - \frac{\mathcal{M}_1^2}{\mathcal{M}_0}\right) \qquad \text{and} \qquad S^3\Pi^{(0)} = |\mathcal{F}||\Lambda|\left(\frac{\mathcal{M}_0\mathcal{M}_3}{\mathcal{M}_1} - \frac{\mathcal{M}_1^2}{\mathcal{M}_0}\right). \tag{5.17}$$

As expected, in a U-shaped channel, these two quantities vanish.

To ensure the asymptotic expansions (5.16), we suggest the introduction of new source terms in the model, designed to relax the enstrophy and the potential towards their respective zeroth-order expansions. These source terms cannot be added to the energy equation, since its current form is necessary to recover the first-order approximation of the discharge.

In addition, the new relaxation source terms shall have to be independent of Λ, since Λ contains H_{ξ_1}. Therefore, the naive choice which consists in simply adding a source term under the form $\frac{J_0}{\varepsilon F^2}(\Psi^{(0)} - \Psi)$ is not advisable, since $\Psi^{(0)}$, given by (5.17), contains Λ. This remark also holds for $\Pi^{(0)}$. To address this issue, we mimic the way the friction term $\mathcal{J}$ was defined to introduce $\mathcal{J}_\Psi$ and $\mathcal{J}_\Pi$, given by:

$$\mathcal{J}_\Psi = |\mathcal{F}|\Lambda\frac{\Psi}{\Psi^{(0)}} = \mathrm{sgn}(Q)|\mathcal{F}||\Lambda|\frac{\Psi}{\Psi^{(0)}} \qquad \text{and} \qquad \mathcal{J}_\Pi = |\mathcal{F}|\Lambda\frac{\Pi}{\Pi^{(0)}} = \mathrm{sgn}(Q)|\mathcal{F}||\Lambda|\frac{\Pi}{\Pi^{(0)}}.$$

According to the definitions (5.17), $\mathcal{J}_\Psi$ and $\mathcal{J}_\Pi$ are indeed independent of Λ. In addition, we have replaced $\mathrm{sgn}(\Lambda)$ with $\mathrm{sgn}(Q)$ since $\mathrm{sgn}(\Lambda) = \mathrm{sgn}(Q^{(0)}) = \mathrm{sgn}(Q)$ for small enough $\frac{\varepsilon F^2}{J_0}$.

Then, we add the following relaxation term to the discharge equation:

$$\frac{J_0}{\varepsilon F^2}SK_1|\mathcal{F}|\Lambda\left(1 - \frac{\Psi}{\Psi^{(0)}}\right) = \frac{J_0}{\varepsilon F^2}SK_1(|\mathcal{F}|\Lambda - \mathcal{J}_\Psi) = \frac{J_0}{\varepsilon F^2}SK_1(\mathcal{I} - \mathcal{J}_\Psi) - K_1\frac{SH_{\xi_1}}{F^2}, \tag{5.18}$$

where K_1 is a nonzero function of S, Q, Ψ and Π, to be determined. This term ensures that Ψ relaxes towards $\Psi^{(0)}$ when $\frac{\varepsilon F^2}{J_0}$ goes to 0, whatever the value of K_1, but it adds a differential term in H_{ξ_1}.

We now have to relax Π towards $\Pi^{(0)}$ when $\frac{\varepsilon F^2}{J_0}$ goes to 0, using only the fourth equation of the system. To avoid adding another differential term in H_{ξ_1} and to retain the stationary wave, we add the following relaxation term to the fourth equation:

$$\frac{J_0}{\varepsilon F^2}QK_2|\mathcal{F}|\Lambda\left(\frac{\Psi}{\Psi^{(0)}} - \frac{\Pi}{\Pi^{(0)}}\right) = \frac{J_0}{\varepsilon F^2}QK_2(\mathcal{J}_\Psi - \mathcal{J}_\pi), \tag{5.19}$$

where K_2 is another nonzero function of S, Q, Ψ and Π, to be determined. Let us emphasize that, for all $K_1 \neq 0$ and $K_2 \neq 0$, the additional terms (5.18) and (5.19) respectively relax Ψ towards $\Psi^{(0)}$ and Π towards $\Pi^{(0)}$.

We thus modify (5.14) as follows:

$$\begin{cases} S_t + Q_{\xi_1} = 0, & \text{(5.20a)} \\ Q_t + \left(\dfrac{Q^2}{S} + P\right)_{\xi_1} + K_1\dfrac{SH_{\xi_1}}{F^2} = P^{lat} + \dfrac{J_0}{\varepsilon F^2}S(\mathcal{I} - \mathcal{J} + K_1(\mathcal{I} - \mathcal{J}_\Psi)), & \text{(5.20b)} \\ E_t + \left(\dfrac{Q}{S}(E + e + P)\right)_{\xi_1} = \dfrac{J_0}{\varepsilon F^2}Q(\mathcal{I} - \mathcal{J}), & \text{(5.20c)} \\ e_t = \dfrac{J_0}{\varepsilon F^2}QK_2(\mathcal{J}_\Psi - \mathcal{J}_\Pi). & \text{(5.20d)} \end{cases}$$

The above model is equivalent, in variables (S, Q, Ψ, Π), to the following one:

$$\begin{cases} S_t + Q_{\xi_1} = 0, & \text{(5.21a)} \\ Q_t + \left(\dfrac{Q^2}{S} + S^3\Psi\right)_{\xi_1} + (1+K_1)\dfrac{SH_{\xi_1}}{F^2} = \dfrac{J_0}{\varepsilon F^2} S(\mathcal{I} - \mathcal{J} + K_1(\mathcal{I} - \mathcal{J}_\Psi)), & \text{(5.21b)} \\ \left(\dfrac{1}{2}\dfrac{Q^2}{S} + \dfrac{1}{2}S^3\Psi\right)_t + \left(\dfrac{Q}{S}\left(\dfrac{1}{2}\dfrac{Q^2}{S} + \dfrac{1}{2}S^3\Pi\right)\right)_{\xi_1} + \dfrac{QH_{\xi_1}}{F^2} = \dfrac{J_0}{\varepsilon F^2} Q(\mathcal{I} - \mathcal{J}), & \text{(5.21c)} \\ \left(\dfrac{1}{2}S^3(\Pi - 3\Psi)\right)_t = \dfrac{J_0}{\varepsilon F^2} Q K_2(\mathcal{J}_\Psi - \mathcal{J}_\Pi). & \text{(5.21d)} \end{cases}$$

To summarize, from the zeroth-order asymptotic expansion of (5.21c), we immediately recover $|\mathcal{F}|\Lambda = \mathcal{J}$, and thus $Q = Q^{(0)}$. Then, from the zeroth-order asymptotic expansion of (5.21b), we get $|\mathcal{F}|\Lambda = \mathcal{J}_\Psi$, i.e. $\Psi = \Psi^{(0)}$. Afterwards, the zeroth-order expansion of (5.21d) ensures that $|\mathcal{F}|\Lambda = \mathcal{J}_\Pi$, which yields $\Pi = \Pi^{(0)}$. Thus, the three required zeroth-order asymptotic expansions are recovered. In addition, it turns out that the first-order expansion of (5.21c) instantly recovers the correct formula for $Q^{(1)}$. Therefore, the model (5.21) (or, equivalently, (5.20)) ensures the required asymptotic expansions (5.16), whatever the choice of K_1 and K_2.

5.3 Mathematical properties of the model; comparison with the classical shallow water system

Equipped with the model (5.20) (or equivalently (5.21)), we are now able to check its mathematical properties, as well as perform a theoretical comparison with the classical shallow water system. In addition, we need to fix the values of the – so far – arbitrary functions K_1 and K_2.

We first note that, unfortunately, the addition of the term $K_1 SH_{\xi_1}/F^2$ in (5.20b) prevents us from rewriting the system under an Euler-like form, since the pressure in (5.20b) would be different from the one in (5.20c). However, we are able to use the almost-Euler-like underlying structure to our advantage in the next developments.

To simplify the forthcoming analysis, we note that $S_{\xi_1} = L(H)H_{\xi_1}$ to rewrite the system (5.21) under the non-conservative form $W_t + A(W)W_{\xi_1} = R(W)$, with $W = (S, U, S^3\Psi, S^3\Pi)^T$, and where the flux matrix $A(W)$ and source terms vector $R(W)$ are given by

$$A(W) = \begin{pmatrix} U & S & 0 & 0 \\ \dfrac{1+K_1}{L(H)F^2} & U & \dfrac{1}{S} & 0 \\ \dfrac{-2SUK_1}{L(H)F^2} & S^3\Pi & -2U & U \\ \dfrac{-6SUK_1}{L(H)F^2} & 3S^3\Pi & -6U & 3U \end{pmatrix} \quad \text{and} \quad R(W) = \frac{J_0}{\varepsilon F^2} \begin{pmatrix} 0 \\ \mathcal{I} - \mathcal{J} + K_1(\mathcal{I} - \mathcal{J}_\Psi) \\ -2SUK_1(\mathcal{I} - \mathcal{J}_\Psi) \\ 2SU[K_2(\mathcal{J}_\Psi - \mathcal{J}_\Pi) - 3K_1(\mathcal{I} - \mathcal{J}_\Psi)] \end{pmatrix}.$$

5.3.1 Hyperbolicity and algebraic properties

For comparison purposes, recall that the characteristic velocities of the classical shallow water system in (S, Q) variables are

$$U \pm \sqrt{\frac{S}{F^2 L(H)}}.$$

In addition, the two characteristic fields associated to these characteristic velocities are genuinely nonlinear.

As stated in Section 5.2.2, before adding the relaxation source term for Ψ, i.e. for $K_1 = 0$, the characteristic velocities of the four-equation model were

$$0,\ \lambda_U = U,\ \lambda_\pm = U \pm \sqrt{\frac{S}{F^2 L(H)} + S^2\Pi}.$$

The characteristic fields associated to 0 and U were linearly degenerate, while the other two characteristic fields were genuinely nonlinear. Straightforward computations show that this system was hyperbolic as soon as $S \neq 0$, and strictly hyperbolic as soon as $S \neq 0$ and $U \neq 0$.

Now, because of the relaxation terms, the characteristic velocities of the system (5.20), i.e. the eigenvalues of the matrix $A(W)$, can no longer be written under a tractable form. Thanks to (5.20d), 0 is still a characteristic velocity of this system. In order to get a better idea of the other three eigenvalues, we perform an asymptotic expansion with respect to the small Froude number F. Let us denote by $\chi_{A(W)}(\lambda)$ the characteristic polynomial of the matrix $A(W)$. After tedious but straightforward computations, we prove that the following asymptotic expansions of λ ensure that $\chi_{A(W)}(\lambda) = \mathcal{O}(F^2)$:

$$\lambda_U^{K_1} = U\frac{1+3K_1}{1+K_1} + \mathcal{O}(F^2),$$
$$\lambda_\pm^{K_1} = \frac{U}{1+K_1} \pm \sqrt{\frac{S}{L(H)}}\left(\frac{\sqrt{1+K_1}}{F} + \frac{F}{2}\frac{S^2\Pi + K_1(2S^2\Pi + K_1(S^2\Pi - 3U^2))}{(1+K_1)^{5/2}}\right) + \mathcal{O}(F^2).$$

Note that, if $K_1 = 0$, we recover the characteristic velocities λ_U and $\lambda_\pm$. In addition, for the system to be hyperbolic, these eigenvalues have to take real values. Therefore, for small enough F, a necessary condition for the hyperbolicity is $1 + K_1 > 0$, and we need to determine K_1 with this constraint in mind.

5.3.2 Linear stability

Let us proceed with determining suitable K_1 and K_2. To that end, we perform a linear stability analysis of the system (5.21). We linearize this system around the equilibrium state $W_0 = (S_0, U_0, S^3\Psi_0, S^3\Pi_0)^T$ such that $R(W_0) = 0$, that is to say

$$U_0 = \frac{Q^{(0)}}{S}\sqrt{\frac{\mathcal{I}}{|\mathcal{F}|\Lambda}} \neq 0, \qquad S^3\Psi_0 = S^3\Psi^{(0)}\frac{\mathcal{I}}{|\mathcal{F}|\Lambda} \qquad \text{and} \qquad S^3\Pi_0 = S^3\Pi^{(0)}\frac{\mathcal{I}}{|\mathcal{F}|\Lambda}.$$

Note that W_0 does not depend on Λ. For the sake of simplicity, let us temporarily assume that $Q^{(0)}$, $\Psi^{(0)}$ and $\Pi^{(0)}$ do not depend on S. This assumption, although false in the general case, allows us to greatly simplify the analysis and to set a framework for the S-dependent case.

To perform a linear stability analysis, we consider the eigenvalues $(\omega_l)_{1\leq l\leq 4}$ of the matrix $M(k) := kA(W_0) + i\boldsymbol{\nabla}_W R(W)$, for all $k \in \mathbb{R}$. The system will be linearly stable if, for each $l \in [\![1,4]\!]$, $\operatorname{Im}\omega_l \leq 0$. For the four-equation model (5.21), the matrix $M(k)$ is given by:

$$M(k) = \begin{pmatrix} kU_0 & kS_0 & 0 & 0 \\ \frac{k(1+K_1)}{L(H)F^2} & kU_0 - 2i\frac{J_0}{\varepsilon F^2}\frac{\mathcal{I}}{U_0} & \frac{k}{S} - i\frac{J_0}{\varepsilon F^2}K_1\frac{\mathcal{I}}{S^3\Psi_0} & 0 \\ \frac{-2kSU_0K_1}{L(H)F^2} & k\frac{S^3\Pi_0}{\mathcal{I}} & -2kU_0 + 2i\frac{J_0}{\varepsilon F^2}K_1\frac{SU_0}{S^3\Psi_0} & kU_0 \\ \frac{-6kSU_0K_1}{L(H)F^2} & 3k\frac{S^3\Pi_0}{\mathcal{I}} & -6kU_0 + 2i\frac{J_0}{\varepsilon F^2}(K_2+3K_1)\frac{SU_0}{S^3\Psi_0} & 3kU_0 - 2i\frac{J_0}{\varepsilon F^2}K_2\frac{SU_0}{S^3\Pi_0} \end{pmatrix}.$$

Let us start with the case $k = 0$, where we can exactly compute the eigenvalues, to get the following expressions:

$$\omega_1^{(0)} = 0, \quad \omega_2^{(0)} = -2i\frac{J_0}{\varepsilon F^2}\frac{\mathcal{I}}{U_0}, \quad \omega_3^{(0)} = 2i\frac{J_0}{\varepsilon F^2}K_1\frac{SU_0}{S^3\Psi_0}, \quad \omega_4^{(0)} = -2i\frac{J_0}{\varepsilon F^2}K_2\frac{SU_0}{S^3\Pi_0}. \tag{5.22}$$

The first two eigenvalues, $\omega_1^{(0)}$ and $\omega_2^{(0)}$, correspond to the ones of the classical shallow water system, and we get two additional ones related to the relaxation source terms. Since $\mathrm{sgn}(U_0) = \mathrm{sgn}(Q^{(0)}) = \mathrm{sgn}(\mathcal{I})$ in the usual range of applications, both shallow water eigenvalues have a non-positive imaginary part. Then, a natural simplification of the other two eigenvalues consists in taking K_1 and K_2 such that $\omega_3^{(0)}$ and $\omega_4^{(0)}$ become equal to $\omega_2^{(0)}$, as follows:

$$K_1 = -\frac{S^3\Psi_0}{SU_0^2} = -\frac{S^4\Psi^{(0)}}{(Q^{(0)})^2} \quad \text{and} \quad K_2 = \frac{S^3\Pi_0}{SU_0^2} = \frac{S^4\Pi^{(0)}}{(Q^{(0)})^2}. \tag{5.23}$$

With this choice, we immediately obtain that all four eigenvalues (5.22) have a non-positive imaginary part.

However, this case $k = 0$ only yields necessary conditions for the linear stability, and we need to take care of the case of a nonzero k. After tedious computations, we get two eigenvalues $\omega_l = \frac{J_0}{\varepsilon F^2}\sum_{j=0}^{3}\omega_l^{(j)}$, for $l \in \{1, 2\}$, such that $\chi(k, \omega_l) = \mathcal{O}((\frac{\varepsilon F^2}{J_0})^3)$, where $\omega \mapsto \chi(k, \omega)$ is the characteristic polynomial of $M(k)$. For the sake of conciseness, we do not write their expressions here. These eigenvalues have a negative imaginary part (i.e. the system is asymptotically linearly stable) as soon as the following condition is satisfied:

$$U_0^2 < \frac{4S_0}{L(H)} + S^2\Pi. \tag{5.24}$$

This condition can be compared to the asymptotic linear stability condition for the shallow water equations, which reads $U_0^2 < 4S_0/L(H)$. Note that, since $\Pi \geq 0$, the linear stability condition for the four-equation model is less restrictive than that of the shallow water equations.

Lastly, recall that we had assumed that $U^{(0)}$, $\Psi^{(0)}$ and $\Pi^{(0)}$ did not depend on S. We now address the real case where these quantities depend on S. To shorten the notations, let us introduce $\mathfrak{c}(S)$ such that $\mathcal{J} = U|U|/(S\mathfrak{c})$, $\Psi_S^{(0)} = \partial\Psi^{(0)}/\partial S$ and $\Pi_S^{(0)} = \partial\Pi^{(0)}/\partial S$. Under the condition (5.24), we obtain the following additional sufficient condition on S for the asymptotic linear stability of the four-equation model:

$$\mathfrak{c}^2\left(3\Psi_S^{(0)} - 2\Pi_S^{(0)}\right) + S^2\left(U^{(0)}\right)^2\mathfrak{c}_S^2 + \left(2S\left(U^{(0)}\right)^2 - \Pi^{(0)} + S\Psi_S^{(0)}\right)\mathfrak{c}\mathfrak{c}_S < 0.$$

As a conclusion, the final hyperbolic four-equation model prescribed by this linear stability analysis is:

$$\begin{cases} S_t + Q_{\xi_1} = 0, \\ Q_t + \left(\dfrac{Q^2}{S} + S^3\Psi\right)_{\xi_1} + \left(1 - \dfrac{S^4\Psi^{(0)}}{(Q^{(0)})^2}\right)\dfrac{SH_{\xi_1}}{F^2} = \dfrac{J_0}{\varepsilon F^2}S\left(\mathcal{I} - \mathcal{J} - \dfrac{S^4\Psi^{(0)}}{(Q^{(0)})^2}(\mathcal{I} - \mathcal{J}_\Psi)\right), \\ \left(\dfrac{1}{2}\dfrac{Q^2}{S} + \dfrac{1}{2}S^3\Psi\right)_t + \left(U\left(\dfrac{1}{2}\dfrac{Q^2}{S} + \dfrac{1}{2}S^3\Pi\right)\right)_{\xi_1} + \dfrac{QH_{\xi_1}}{F^2} = \dfrac{J_0}{\varepsilon F^2}Q(\mathcal{I} - \mathcal{J}), \\ \left(\dfrac{1}{2}S^3(\Pi - 3\Psi)\right)_t = \dfrac{J_0}{\varepsilon F^2}Q\dfrac{S^4\Pi^{(0)}}{(Q^{(0)})^2}(\mathcal{J}_\Psi - \mathcal{J}_\Pi). \end{cases} \tag{5.25}$$

The study of the linear stability of the system (5.25) is thus complete. Regarding its hyperbolicity, recall that it is hyperbolic under the condition $1 + K_1 > 0$ for small enough F. With K_1 given by (5.23), this condition becomes $S^3\Psi^{(0)} < (Q^{(0)})^2/S$. According to the definition (5.10) of $S^3\Psi$, this is equivalent to

$$\int_{\Xi_-}^{\Xi_+} h(u^{(0)})^2\, d\xi_2 < 2S(U^{(0)})^2,$$

where $U^{(0)} = Q^{(0)}/S$. This condition is satisfied in the regimes under consideration. As a consequence, the system (5.25) is hyperbolic.

6 Validation of the four-equation model

The four-equation model (5.25) has been built in order to possess the required consistency properties. This last section is devoted to the numerical validation of our four-equation model. In its first part, we present some reference solutions, as well as the numerical schemes we use to approximate these solutions. The second part of this section is then dedicated to the numerical experiments themselves.

In this section, we will consider the three 1D models at our disposal:

- the classical shallow water model, later referred to as SW, given by (1.1), which is consistent only when considering U-shaped channels;
- the shallow water model equipped with the friction term (5.2), later referred to as A0, consistent with the zeroth-order asymptotic expansion of Q;
- the four-equation model (5.25), later referred to as A1, consistent with the first-order asymptotic expansion of Q.

The goal of this section is to compare the results of the three models under consideration. We expect the SW model to be inconsistent as soon as the channel is not U-shaped. Moreover, we also expect that the A1 model should yield more accurate results than the A0 one.

6.1 Reference solutions and numerical considerations

We begin by discussing the theory of the backwater curves (i.e. the stationary solutions) of the three 1D models at our disposal. Then, we introduce the manufactured stationary 2D reference solution that will be used to perform several stationary numerical experiments. Lastly, we present the numerical discretization used throughout the experiments.

6.1.1 Backwater curves in 1D

We first consider the backwater curves of the 1D models under consideration (i.e. its stationary solutions, free from time). For the classical shallow water system in (S, Q) variables (1.1), they are given by a constant discharge $Q = Q_0$ and the profile equation

$$H_{\xi_1} = \frac{J_0}{\varepsilon} \frac{\mathcal{I} - \mathcal{J}_{SW}}{1 - F^2 L(H) \dfrac{Q_0^2}{S^3}}, \tag{6.1}$$

where the friction model $\mathcal{J}_{SW}$ is given by

$$\mathcal{J}_{SW} = \frac{Q_0 |Q_0|}{H^{2+p} c_{SW}^2}$$

As ε / J_0 goes to 0, the backwater curves become driven only by the numerator of the H_{ξ_1} equation. More specifically, H will be equal to H_n^{SW}, defined as the value of H canceling the numerator $\mathcal{I} - \mathcal{J}_{SW}$ for a uniform flow. This quantity H_n is referred to as the normal height in the hydraulic literature. Thus, we get

$$H_n^{SW} = \left(\frac{Q_0 |Q_0|}{\mathcal{I}\, c_{SW}^2} \right)^{\frac{1}{2+p}}.$$

For the A0 model, the only difference is the friction model, and the backwater equation reads

$$H_{\xi_1} = \frac{J_0}{\varepsilon} \frac{\mathcal{I} - \mathcal{J}}{1 - F^2 L(H) \dfrac{Q_0^2}{S^3}}, \tag{6.2}$$

instead of (6.1). Therefore, we note that the value of the normal height depends on the friction model $\mathcal{J}$ under consideration, given by (5.4): $\mathcal{J}$ depends on S, and thus on H. The normal height H_n^{A0} is now implicitly defined as the value of H canceling $\mathcal{I} - \mathcal{J}$.

The backwater curves of the four-equation model (5.25), in addition to the constant discharge $Q = Q_0$, read as follows:

$$\begin{cases} H_{\xi_1} = \dfrac{J_0}{\varepsilon} \dfrac{\mathcal{I} - \mathcal{J} - \dfrac{F^2}{2S}\left(S^3\Pi\right)_{\xi_1}}{1 - F^2 L(H)\left(\dfrac{Q_0^2}{S^3} + \dfrac{S^3\Pi}{2S^2}\right)}, \\ (S^3\Psi)_{\xi_1} = \dfrac{J_0}{\varepsilon F^2} S\left(\mathcal{I} - \mathcal{J} - \dfrac{S\Psi^{(0)}}{(Q^{(0)})^2}(\mathcal{I} - \mathcal{J}_\Psi)\right) - \left(1 - \dfrac{S\Psi^{(0)}}{(Q^{(0)})^2} - F^2 L(H)\dfrac{Q_0^2}{S^3}\right)\dfrac{SH_{\xi_1}}{F^2}, \\ \dfrac{\Psi}{\Psi^{(0)}} = \dfrac{\Pi}{\Pi^{(0)}}. \end{cases} \tag{6.3}$$

We note that the normal height H_n^{A1} associated to the four-equation model is also defined by $\mathcal{I} - \mathcal{J} = 0$. However, the backwater curve for the four-equation model contains an additional $\mathcal{O}(F^2)$ term compared to the one of the shallow water model. This additional term comes from the fact that we ensure a first-order approximation on the discharge.

6.1.2 Steady 2D reference solution

In the forthcoming developments, we consider a stationary solution of the 2D equations (2.3) in the weakly meandering asymptotic regime, characterized by $R_y = \mathcal{O}(\frac{\varepsilon F^2}{J_0})$, $R_l = \mathcal{O}(\frac{\varepsilon F^2}{J_0})$ and $\frac{\varepsilon F^2}{J_0} \ll 1$. The goal of these computations is to rewrite this system under a computationally tractable form. Thanks to this new form, we will be able to manufacture a steady reference solution, against which the three 1D models will be tested.

Let us begin by writing the unsteady system (2.3) in the asymptotic regime under consideration. Assuming a stationary solution and a weakly meandering river, (2.3) becomes:

$$\begin{cases} (\tilde{h}v_1)_{\xi_1} + (\tilde{h}v_2)_{\xi_2} = 0, & \text{(6.4a)} \\ v_1(v_1)_{\xi_1} + v_2(v_1)_{\xi_2} + \dfrac{1}{|\mathcal{F}|^2 F^2}(h_{\xi_1} + \phi_{\xi_1}) = \dfrac{J_0}{\varepsilon F^2}\left(\dfrac{\mathcal{I}}{|\mathcal{F}|^2} - \dfrac{|\mathcal{F}|v_1|v_1|}{(1+c)^2 h^p}\right) + \mathcal{O}\left(\dfrac{\varepsilon F^2}{J_0}\right), & \text{(6.4b)} \\ h_{\xi_2} + \phi_{\xi_2} = \mathcal{O}\left(\left(\dfrac{\varepsilon F^2}{J_0}\right)^2\right). & \text{(6.4c)} \end{cases}$$

The first step to solve this system is to note that (6.4a) imposes that the discharge be divergence-free. Therefore, we introduce a discharge potential Φ, such that $\tilde{h}v_1 = \Phi_{\xi_1}$ and $\tilde{h}v_2 = \Phi_{\xi_2}$. In this context, the equation (6.4a) is equivalent to $\Delta\Phi = 0$. We prescribe suitable boundary conditions, ensuring that $\tilde{h}v_2 = \mathcal{O}(\frac{\varepsilon F^2}{J_0})$ to satisfy the asymptotic regime. Numerically solving this first equation gives the quantities $\tilde{h}v_1$ and $\tilde{h}v_2$.

Now, we need to compute $h(\xi_1, \xi_2)$. Since $\tilde{h}v_2 = \mathcal{O}(\frac{\varepsilon F^2}{J_0})$, (6.4b) becomes

$$\frac{|\mathcal{F}|v_1|v_1|}{(1+c)^2 h^p} = \frac{\Lambda}{|\mathcal{F}|} - \frac{\varepsilon F^2}{J_0} v_1(v_1)_{\xi_1} + \mathcal{O}\left(\left(\frac{\varepsilon F^2}{J_0}\right)^2\right). \tag{6.5}$$

We look for a non-uniform Chézy coefficient $c(\xi_1, \xi_2)$, which therefore becomes an unknown of the problem. At this level, we have two unknowns, $h(\xi_1, \xi_2)$ and $c(\xi_1, \xi_2)$.

To address this issue, let us use both the divergence-free discharge and the asymptotic regime. First, we get from (6.5) the equation on c, as follows:

$$(1+c)^2 = \frac{|\mathcal{F}|^2 q|q|h^{1-p}}{|\mathcal{F}|^2 \Lambda h^3 - \dfrac{\varepsilon F^2}{J_0} q\left(\tilde{h}q_{\xi_1} - q\tilde{h}_{\xi_1}\right)} + \mathcal{O}\left(\left(\frac{\varepsilon F^2}{J_0}\right)^2\right), \tag{6.6}$$

where the already computed quantity $\tilde{h}v_1$ is denoted by q. Then, we replace the velocities in (6.5) by their asymptotic expansions. Therefore, the equation (6.5) becomes

$$\frac{\varepsilon F^2}{J_0}\left(v_1^{(0)}\left(v_1^{(0)}\right)_{\xi_1} + \frac{2|\mathcal{F}|v_1^{(1)}|v_1^{(0)}|}{(1+c)^2 h^p}\right) = \frac{\Lambda}{|\mathcal{F}|} - \frac{|\mathcal{F}|v_1^{(0)}|v_1^{(0)}|}{(1+c)^2 h^p} + \mathcal{O}\left(\left(\frac{\varepsilon F^2}{J_0}\right)^2\right), \tag{6.7}$$

where the asymptotic expansions $v_1^{(0)}$ and $v_1^{(1)}$ are respectively given by (3.4) and (3.7).

Injecting (6.6) into (6.7) therefore yields an equation whose only unknown is h, and which manufactures the Chézy coefficient such that $h + \phi$ is almost uniform in space. Solving this equation for h allows us to plug this value into (6.6), and therefore to complete the determination of the 2D reference stationary solution, while ensuring that the correct asymptotic regime is satisfied. These computations are made easier by the fact that we have $h_{\xi_2} + \phi_{\xi_2} = 0$.

This process, in addition to the usual reference scaling, requires to fix the values of $\tilde{h}v_1$ and $\tilde{h}v_2$ at the boundaries, as well as an equivalent to the 1D normal height discussed in Section 6.1.1. These three non-dimensional quantities will respectively be denoted by $\tilde{h}(v_1)_0$, $\tilde{h}(v_2)_0$, and H_n^{2D}, and numerical values will be given in the relevant Section. In the end, we get a solution whose free surface $H = h + \phi$ will be close to the fixed normal height.

6.1.3 Discretization

We now briefly discuss the numerical discretization of the models under consideration, to be used in the validation numerical experiments of the next part of this Section.

The steady 2D reference solution. Obtaining this 2D reference solution relies on a natural discretization of the set of equations presented in Section 6.1.2. For the sake of simplicity, we use a finite difference method on a Cartesian grid with n_{ξ_1} points in the ξ_1-direction and n_{ξ_2} points in the ξ_2-direction.

The backwater curves. Since the parameter ε/J_0 can become small, stiff terms can appear in the backwater curves given by (6.1), (6.2) and (6.3). Therefore, we adopt a fully implicit finite difference discretization of the three models under consideration. We use a uniform 1D mesh with n_{ξ_1} discretization elements. In addition, for the Chézy coefficient and the topography, an underlying 2D mesh is needed. To address this issue, we use the mesh presented above, with $n_{\xi_1} \times n_{\xi_2}$ points.

The unsteady problem in 1D. Numerical experiments with steady solutions will have convinced us that the SW model is unsuitable as soon as the channel is no longer U-shaped. Therefore, we only consider the A0 and A1 models for 1D unsteady problems. These models are governed by hyperbolic systems of balance laws. In addition, some terms in $\mathcal{O}(\frac{J_0}{\varepsilon F^2})$ and $\mathcal{O}(\frac{1}{F^2})$ are stiff. These two remarks prompt us to propose a finite difference splitting strategy, where the non-stiff part is treated explicitly, and the stiff part is treated implicitly. This amounts to introducing IMEX strategies that are both asymptotic preserving (regarding stiff source terms) and adapted to Low Froude number limits: see e.g. [Bispen et al., 2014] and references therein for more details.

For the A0 model, we denote by $(S_{A0})_i^n$ and $(Q_{A0})_i^n$ the discretizations of the section and the discharge at the spatial node $(\xi_1)_i$ and at time t^n. The first step of the space-time discretization consists in considering the non-stiff part of the A0 system, given by:

$$\begin{cases} S_t + Q_{\xi_1} = 0, \\ Q_t + \left(\dfrac{Q^2}{S}\right)_{\xi_1} = 0. \end{cases}$$

This non-stiff part is discretized explicitly using an upwind flux, as follows:

$$\begin{cases} (S_{A0})_i^{n+\frac{1}{2}} = (S_{A0})_i^n - \dfrac{\Delta t}{\Delta x}\Big((Q_{A0})^n_{i+\frac{1}{2}} - (Q_{A0})^n_{i-\frac{1}{2}}\Big), \\ (Q_{A0})_i^{n+\frac{1}{2}} = (Q_{A0})_i^n - \dfrac{\Delta t}{\Delta x}\left(\left(\dfrac{Q_{A0}^2}{S_{A0}}\right)^n_{i+\frac{1}{2}} - \left(\dfrac{Q_{A0}^2}{S_{A0}}\right)^n_{i-\frac{1}{2}}\right), \end{cases}$$

where the upwind fluxes are given, for any quantity X, by

$$X^n_{i+\frac{1}{2}} = \begin{cases} X_i^n & \text{if } \dfrac{1}{2}\big((Q_{A0})_i^n + (Q_{A0})_{i+1}^n\big) > 0, \\ X_{i+1}^n & \text{otherwise,} \end{cases}$$

where Δx is the space step, and where Δt is the time step, related to Δx through a usual CFL-like condition (see e.g. [LeVeque, 2007]), and such that $\Delta t = \mathcal{O}(\Delta x)$. The intermediate values $(S_{A0})_i^{n+\frac{1}{2}}$ and $(Q_{A0})_i^{n+\frac{1}{2}}$ are then used as initial conditions for the stiff part of the A0 system, given by:

$$\begin{cases} S_t = 0, \\ Q_t + \dfrac{SH_{\xi_1}}{F^2} = \dfrac{J_0}{\varepsilon F^2} S\left(\mathcal{I} - |\mathcal{F}|\Lambda \dfrac{Q|Q|}{Q^{(0)}|Q^{(0)}|}\right). \end{cases}$$

We immediately note that S, and therefore H, is time-independent in this stiff second step. Therefore, we obtain $(S_{A0})_i^{n+1} = (S_{A0})_i^{n+\frac{1}{2}}$. Recalling the friction model (5.2) and noting that $\mathrm{sgn}(Q) = \mathrm{sgn}(Q^{(0)})$ for small enough $\frac{\varepsilon F^2}{J_0}$, the updated discharge is then given by the ODE

$$Q_t = \frac{J_0}{\varepsilon F^2} S|\mathcal{F}|\Lambda\left(1 - \frac{Q^2}{(Q^{(0)})^2}\right),$$

whose only unknown is Q. Integrating this ODE between times 0 and t, we get the following exact expression for Q:

$$Q(t) = Q^{(0)} \frac{\tanh\left(\dfrac{J_0}{\varepsilon F^2}\dfrac{S|\mathcal{F}||\Lambda|}{|Q^{(0)}|}t\right) + \dfrac{Q(0)}{Q^{(0)}}}{1 + \tanh\left(\dfrac{J_0}{\varepsilon F^2}\dfrac{S|\mathcal{F}||\Lambda|}{|Q^{(0)}|}t\right)\dfrac{Q(0)}{Q^{(0)}}}.$$

The corresponding discretization reads as follows:

$$(Q_{A0})_i^{n+1} = (Q^{(0)})_i^{n+1} \frac{\tanh\left(\dfrac{J_0}{\varepsilon F^2}\dfrac{(S_{A0})_i^{n+1}(|\mathcal{F}||\Lambda|)_i^{n+1}}{|(Q^{(0)})_i^{n+1}|}\Delta t\right) + \dfrac{(Q_{A0})_i^{n+\frac{1}{2}}}{(Q^{(0)})_i^{n+1}}}{1 + \tanh\left(\dfrac{J_0}{\varepsilon F^2}\dfrac{(S_{A0})_i^{n+1}(|\mathcal{F}||\Lambda|)_i^{n+1}}{|(Q^{(0)})_i^{n+1}|}\Delta t\right)\dfrac{(Q_{A0})_i^{n+\frac{1}{2}}}{(Q^{(0)})_i^{n+1}}},$$

where we recall that Λ and $Q^{(0)}$ only depend on S_{A0} and the node i, and therefore we note that the above equation explicitly determines $(Q_{A0})_i^{n+1}$. In addition, note that we correctly recover $(Q_{A0})_i^{n+1} \to (Q^{(0)})_i^{n+1}$ when $\frac{\varepsilon F^2}{J_0} \to 0$. The presentation of the numerical discretization of the model A0 is thus complete.

For the A1 model, we apply a similar procedure, which we do not write in detail for the sake of conciseness. The main difference between the two discretizations is that the system of ODEs resulting from the stiff part can no longer be exactly solved, and a multivariate nonlinear root-finding algorithm (in practice, Newton's method) has to be applied. In addition, thanks to the splitting procedure, we also correctly recover the discrete first-order asymptotic regime.

The unsteady model in 2D. Finally, to compare unsteady 1D results to a reference solution, we require a numerical scheme for the 2D system (2.2). We elect to use the DASSFLOW code [Couderc et al., 2015, Monnier et al., 2016], designed to solve this system in conservative form and validated on multiple 2D test cases.

6.2 Numerical validation

The second part of this section is devoted to the numerical validation itself. We begin by discussing the chosen geometries and the values we give to the reference dimensionalization parameters. Then, we compare the steady solutions of each 1D model to the stationary 2D reference solution, as well as the unsteady solutions of the 1D models.

6.2.1 Geometry and values of the dimensionalization parameters

For the sake of simplicity, we consider a non-meandering, evenly sloped and symmetrical trapezoidal channel. In addition, to avoid treating dry areas in the discretization, we suppose that the channel is walled and filled with water. The dimensionalization parameters are chosen such that the channel roughly corresponds to the Garonne river upstream of the city of Toulouse.

Geometry. Recall that the topography is given by $Z(\xi_1, \xi_2) = b_0(\xi_1) + \frac{\varepsilon}{I_0}\phi(\xi_1, \xi_2)$. Also, note that $b_0(\xi_1)$ only intervenes through its derivative $(b_0)_{\xi_1}$, which we take equal to 1. Furthermore, we assume that the computational domain is $[0, (\xi_1)_+]$, whose numerical value is given later. For simplicity, we assume that the longitudinal slope is only driven by b_0, and we take $\phi(\xi_1, \xi_2) = \phi(\xi_2)$. Then, we get a symmetrical trapezoidal channel by considering

$$\phi(\xi_2) = \begin{cases} (-\xi_2 - l)\tan\theta & \text{if } \Xi_- < \xi_2 \leq -l, \\ 0 & \text{if } -l \leq \xi_2 \leq l, \\ (\xi_2 - l)\tan\theta & \text{if } l \leq \xi_2 < \Xi_+, \end{cases} \tag{6.8}$$

where the notations are explained in Figure 3, and where we take $\Xi_- = -\Xi_+$. The numerical values of $\Xi_\pm$, l and θ are given in the next paragraph, for each experiment. Note that a U-shaped channel is a specific case of this geometry. Finally, remark that walls are present on each bank of the channel in Figure 3. We introduced these walls to avoid dry areas.

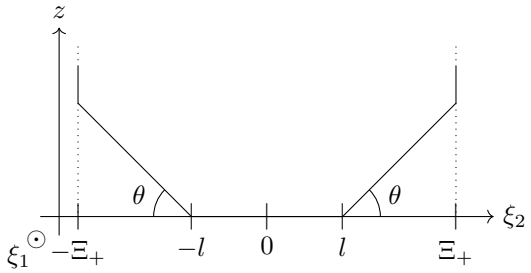

Figure 3: Sketch of the function $\phi(\xi_2)$, i.e. of the channel cross-section.

For the sake of completeness, we finally provide the expression of the channel width $L(z)$, as well as the correspondence between S and H. According to (6.8), we have

$$L(z) = \begin{cases} 2l + \dfrac{2z}{\tan\theta} & \text{if } 0 \leq z \leq (\Xi_+ - l)\tan\theta, \\ 2\Xi_+ & \text{otherwise.} \end{cases}$$

Therefore, since we assume $H > (\Xi_+ - l)\tan\theta$ to avoid dry areas, we get

$$S(H) = \int_0^H L(z)\,dz = 2H\Xi_+ - (\Xi_+ - l)^2 \tan\theta.$$

Values of the reference parameters. We now give, for each of the three experiments performed in the remainder of this Section, the chosen values of the reference parameters in Tables 1 and 2, as well as the geometry and numerical discretization in Table 3. The reference discharge $\mathcal{Q}$ is defined by $\mathcal{Q} = \mathcal{H}\mathcal{U}$. The experiment #1, presented in Section 6.2.2, concerns the simulation of backwater curves. In Table 3, we highlight the two parts of this experiment, #1a and #1b, respectively corresponding to a U-shaped channel and to a trapezoidal channel. The experiment #2, in Section 6.2.3, provides a comparison with the 2D reference solution. The experiment #3, in Section 6.2.4, is the unsteady simulation of a flood. For this experiment, $\mathcal{X}$ is computed according to the characteristic time of the flood. All numerical results will be presented in non-dimensional variables.

parameter	g (m.s^{-2})	p	$\mathcal{X}$ (km)	$\mathcal{Y}$ (m)	$\mathcal{Q}$ (m^3.s^{-1})	I_0	$\mathcal{C}$ (m$^{5/3}$.s^{-1})	F
experiment #1	9.81	4/3	5	45	225	4×10^{-4}	25	0.075
experiment #2	9.81	4/3	10	50	25	1×10^{-3}	20	0.1
experiment #3	9.81	4/3	~ 1.77	90	40	1.6×10^{-3}	45	0.09

Table 1: Values of the reference parameters for each experiment.

parameter	$\mathcal{H}$ (m)	$\mathcal{U}$ (m.s^{-1})	J_0	ε	R_l	$\frac{\varepsilon F^2}{J_0}$
experiment #1	7.68	0.651	4.47×10^{-5}	1.53×10^{-3}	9×10^{-3}	0.193
experiment #2	1.37	0.366	2.21×10^{-4}	1.37×10^{-4}	5×10^{-3}	6.18×10^{-3}
experiment #3	1.35	0.328	3.55×10^{-5}	7.65×10^{-4}	5.08×10^{-2}	0.175

Table 2: Approximate values of the other parameters for each experiment, computed from Table 1.

parameter	$(\xi_1)_+$	n_{ξ_1}	l	θ	Ξ_+	n_{ξ_2}
experiment #1a	5	500	0	0	0.5	100
experiment #1b	5	500	0.25	60	0.5	100
experiment #2	1	200	0.15	60	0.5	20
experiment #3	~ 36.7	400	0.15	45	0.5	40

Table 3: Values of the geometry and discretization parameters for each experiment.

Chézy distribution. For the experiment #1a, we take a uniform Chézy distribution, i.e. $1 + c(\xi_1, \xi_2) = 1$. For the experiment #1b, we set:

$$1 + c(\xi_1, \xi_2) = 1 + 1.99\,\frac{\xi_2 - (\Xi_- + \Xi_+)/2}{\Xi_+ - \Xi_-}.$$

For the experiment #2, the Chézy distribution is algorithmically computed according to the asymptotic regime and to the procedure detailed in Section 6.1.2. Finally, for the experiment #3, we set

$$1 + c(\xi_1, \xi_2) = 1.5 - 2\,\frac{|\xi_2 - (\Xi_- + \Xi_+)/2|}{\Xi_+ - \Xi_-}.$$

6.2.2 Numerical experiment: backwater curves

We start with the simulation of backwater curves, presented in Section 6.1.1, and labeled experiment #1 in Tables 1, 2 and 3. We set the normal height H_n equal to 1, and we compute the uniform and constant discharge Q according to this value of H_n by taking $Q = Q^{(0)}$.

In the first part of this experiment, labeled #1a, we take a U-shaped channel with uniform friction, to get $Q \simeq 2.99$. Then, in experiment #1b, we switch to a trapezoidal channel with non-uniform friction, to get $Q \simeq 2.71$. The corresponding dimensional values are roughly equal to 650 $m^3.s^{-1}$, which characterizes a mild flood regime.

From Section 6.1.1, we note that the backwater curves are governed by a system of ODEs, and thus we only require a single boundary condition on the height, H_0, to drive this steady flow. In practice, we take $H_0 = (H_n + 9H_c)/10$, where H_c is the critical height, defined by canceling the denominator of the H_{ξ_1} equation. For the A1 system, the enstrophy and potential are initialized by taking the values $\Psi^{(0)}$ and $\Pi^{(0)}$ corresponding to H_0. The numerical results are presented in Figure 4.

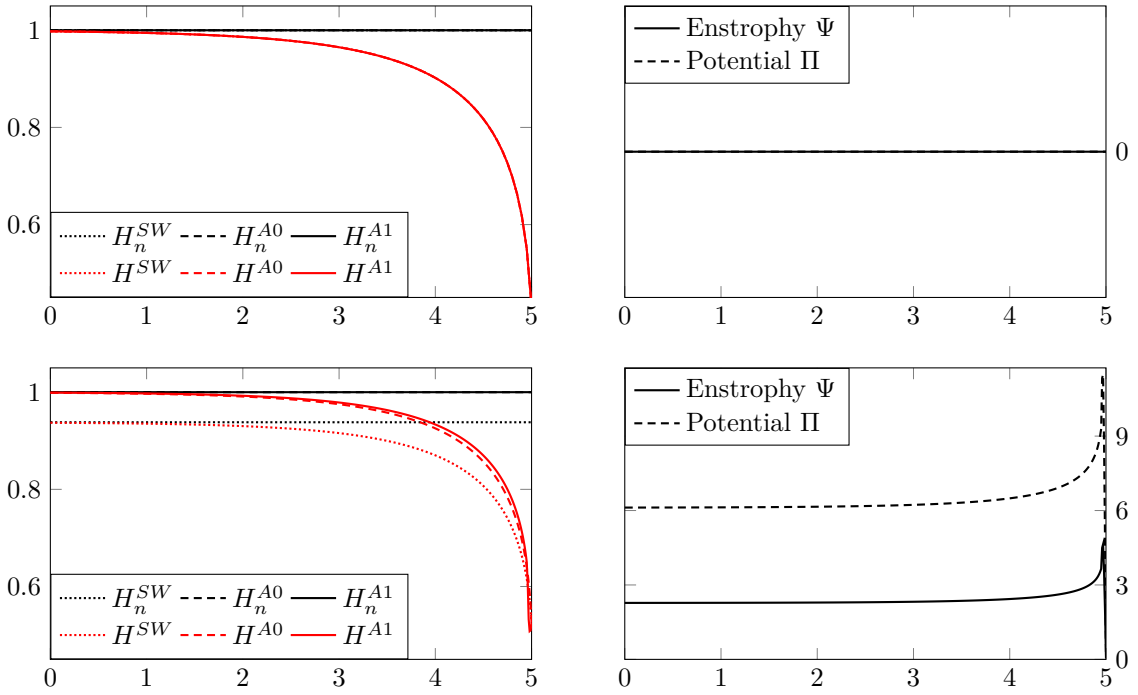

Figure 4: Simulation of backwater curves. Top panels: U-shaped channel with uniform friction. Bottom panels: trapezoidal channel with non-uniform friction. Left panel: height and normal height with respect to the position, for the three models. Right panel: enstrophy Ψ and potential Π for the A1 model.

In the left panels of Figure 4, we have represented the free surface H for the three models, denoted in the legend by H^{SW}, H^{A0} and H^{A1}, as well as the associated normal heights H_n for each model. As expected, we note that the free surface H converges towards the relevant normal height when x goes to 0. Moreover, as explained in Section 6.1.1, this normal height only depends on the friction model. Since we have the same friction model for the A0 and A1 models, the normal height associated to these models are the same, contrary to the one associated to the SW model, unless the channel is U-shaped. By comparing the two left panels of Figure 4, we note that, as expected, the three models give the same results when the channel is U-shaped. However, as soon as it is no longer the case, the SW model greatly differs from the other two, which allows us to conclude that the SW model is irrelevant as soon as the channel is not U-shaped. Finally, note that the backwater curves of the A0 and A1 models are different when the channel is not U-shaped, up to $\mathcal{O}((\frac{\varepsilon F^2}{J_0})^2)$,

as expected.

In the right panels of Figure 4, we have displayed the enstrophy Ψ and the potential Π computed by the A1 model. As expected, these quantities vanish when the channel is U-shaped and the friction is uniform. In addition, once this is no longer the case, we note a similar behavior of these quantities compared to the height, in the sense that they tend towards a constant value when x goes to 0.

6.2.3 Numerical experiment: comparison to 2D steady solution

We now turn to the comparison between the 2D reference steady solution from Section 6.1.2 and the models under consideration.

Recall that the 2D solution is only driven by its boundary conditions $\tilde{h}(v_1)_0$ and $\tilde{h}(v_2)_0$ on the discharge, and that it will produce a steady flow at normal height H_n^{2D}. To compute this reference solution, we take $H_n^{2D} = 1$, $\tilde{h}(v_1)_0 \simeq 0.75$ and $|\tilde{h}(v_2)_0| = \mathcal{O}(\frac{\varepsilon F^2}{J_0})$. These 2D results are presented in Figure 5.

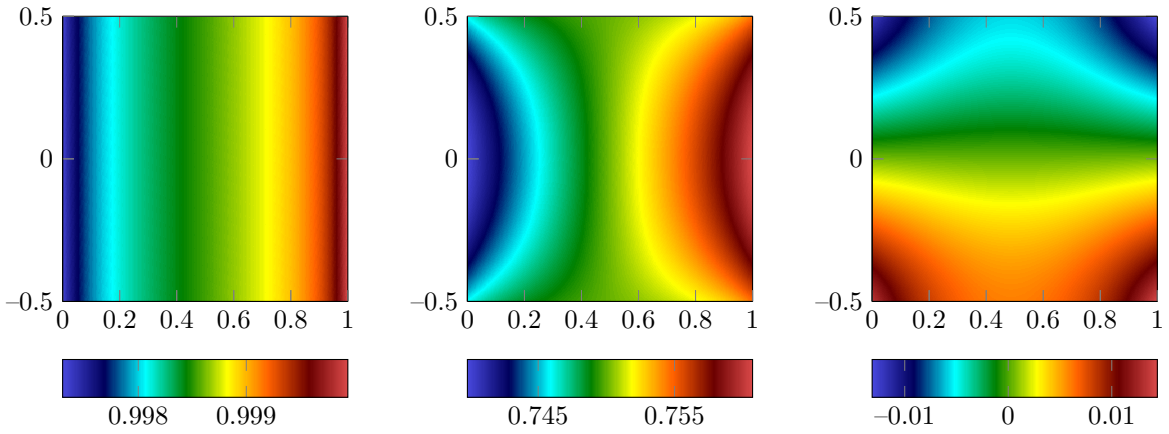

Figure 5: The 2D reference steady solution, computed from the process exhibited in Section 6.1.2. From left to right: free surface $H(\xi_1) = h(\xi_1, \xi_2) + \phi(\xi_2)$, ξ_1-discharge $\tilde{h}v_1(\xi_1, \xi_2)$ and ξ_2-discharge $\tilde{h}v_2(\xi_1, \xi_2)$.

Equipped with this 2D solution, we can compare it to the three 1D models at our disposal. The constant and uniform 1D discharge is defined by $Q = \int_{\Xi_-}^{\Xi_+} \tilde{h}v_1(0.5, y)\, d\xi_2$. In Figure 6, we present the free surface $H(\xi_1)$ computed by the SW (dotted lines), A0 (dashed lines) and A1 (solid lines) models, in addition to the corresponding normal heights.

The left panel of Figure 6 contains these comparisons. We note that the normal height associated to the SW model does not correspond at all to the 2D normal height (we get $H_n^{SW} \simeq 0.736$ while we have set $H_n^{2D} = 1$). Thus, the free surface computed by the classical SW model is once again wildly inconsistent with the reference 2D solution.

Turning to the right panel of Figure 6, which displays a zoom of the left panel around the line $H = 1$, we observe that the A0 and A1 models are consistent with the 2D reference solution. Indeed, the small variations in free surface are due to the uniformity in space of the 1D discharge, compared to the 2D discharge whose divergence vanishes, but whose ξ_1-derivative is nonzero. Moreover, the 2D height becomes very close to the 1D ones around $\xi_1 = 0.5$, since the 1D discharge is the ξ_2-average of the 2D one at point $\xi_1 = 0.5$. We do not observe much difference between the solutions of the A0 and A1 models: the relative error in L^2 norm is around 5×10^{-5}. This was to be expected since $\frac{\varepsilon F^2}{J_0} \simeq 6.18 \times 10^{-3}$ in this experiment, and the difference between the A0 and A1 models is $\mathcal{O}((\frac{\varepsilon F^2}{J_0})^2)$.

Finally, in Figure 7, we display the relative errors in L^2 norm between the enstrophy Ψ (left panel) or the potential Π (right panel), computed by the A1 model, and their zeroth- and first-order approximations. As expected, these errors are $\mathcal{O}((\frac{\varepsilon F^2}{J_0})^2)$, since the A1 model is consistent up to $\mathcal{O}(\frac{\varepsilon F^2}{J_0})$ in Ψ and Π.

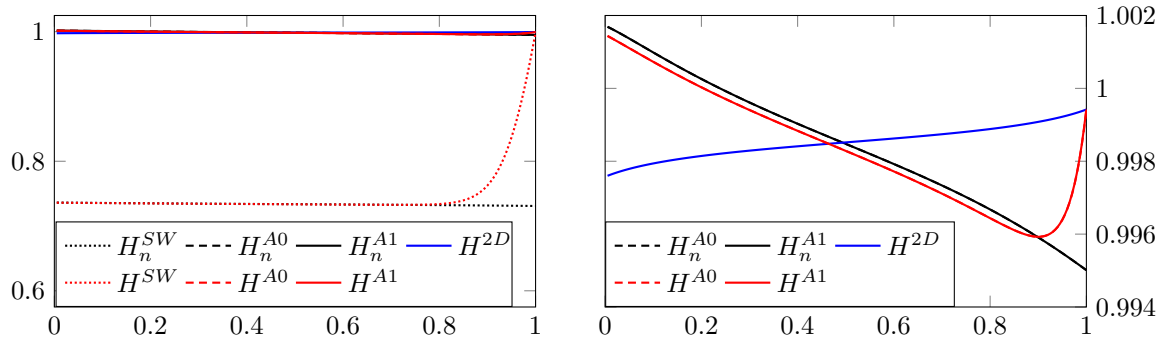

Figure 6: Comparison with the 2D steady reference solution. Left panel: height and normal height with respect to the position, for the three models; comparison with the 2D height. Right panel: zoom on the left panel to highlight the differences between the 2D height and the one computed by the A0 and A1 models.

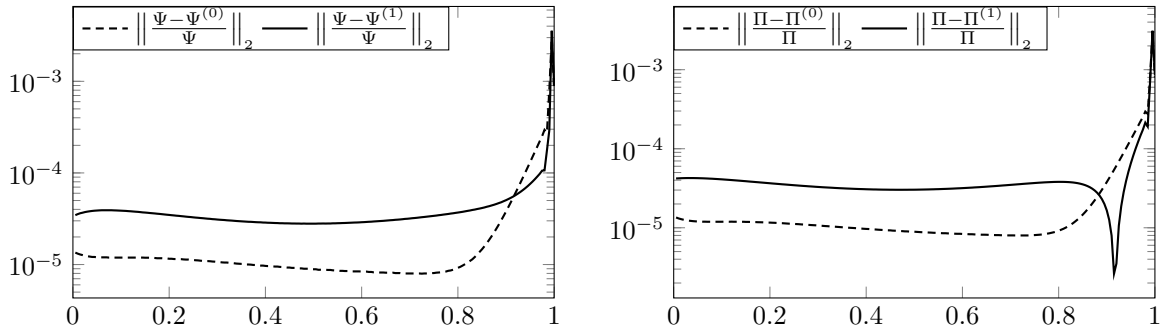

Figure 7: Errors between the computed enstrophy (left panel) or potential (right panel) and their zeroth- and first-order expansions, computed using the A1 model.

6.2.4 Numerical experiment: unsteady flood flow

In this final experiment, we consider the unsteady case of a flood. The reference solution is given by the DASSFLOW code [Couderc et al., 2015, Monnier et al., 2016]. Since the SW model has been proven to be inconsistent by the previous two experiments, we no longer consider it. We compare the A0 and A1 models, discretized as explained in Section 6.1.3, to the reference solution.

In addition, we consider the kinematic waves (KW) approximation, which consists in taking the mass conservation equation of the shallow water equations and considering $Q = Q^{(0)}(S)$, as follows:

$$S_t + (Q^{(0)}(S))_{\xi_1} = 0.$$

Since $Q^{(0)}$ depends nonlinearly on Λ, it depends on S_{ξ_1}. The kinematic wave equation therefore is a nonlinear diffusion equation, which we discretize with a classical upwind scheme. Note that this numerical scheme involves a restrictive stability condition on the time step, in $\Delta t = \mathcal{O}(\Delta x^2)$.

The reference parameters for this experiment correspond to the Garonne river upstream of Toulouse (see Tables 1 and 3). We consider a flood lasting a dimensional time of 7.5h, and the total dimensional time of the unsteady experiment is 10h. The discharge increases during the dimensional time $T = 1.5$h, then stagnates during the dimensional time 1.5h, and finally decreases to the initial level during the dimensional time 4.5h. We get the characteristic length $\mathcal{X}$ from the characteristic flood time T by setting $\mathcal{X} = \mathcal{U}T \simeq 1.772$km. The total dimensional length is 65km ($\xi_1 \in [0, 65/\mathcal{X}]$, where $65/\mathcal{X} \simeq 36.69$), and we consider a probe at dimensional position 62.25km ($\xi_1 \simeq 34.57$). This domain roughly corresponds to the Marquefave-Toulouse portion of the Garonne river.

The free surface is initialized at the normal height. From this normal height, we compute the initial discharge Q_n, enstrophy and potential through their respective zeroth-order asymptotic expansions. As a consequence, the flow of water in the river is a steady solution before the flood begins. The flood itself is simulated by a time-dependent left boundary condition on the discharge Q. We take $Q(t,0) = Q_{in}(t)$, with

$$Q_{in}(t) = \begin{cases} Q_n + \left(\dfrac{2200}{\mathcal{Q}} - Q_n\right)\dfrac{t}{0.15\,t_{end}} & \text{if } t \leq 0.15\,t_{end}, \\ \dfrac{2200}{\mathcal{Q}} & \text{if } 0.15\,t_{end} \leq t \leq 0.30\,t_{end}, \\ Q_n + \left(\dfrac{2200}{\mathcal{Q}} - Q_n\right)\dfrac{0.75\,t_{end} - t}{0.75\,t_{end} - 0.30\,t_{end}} & \text{if } 0.30\,t_{end} \leq t \leq 0.75\,t_{end}, \\ Q_n & \text{otherwise,} \end{cases}$$

where t_{end} is the non-dimensional final time. This boundary condition ensures a dimensional peak flood discharge of $2200\text{m}^3.\text{s}^{-1}$, which corresponds to a 5-year flood for the Garonne river. The left boundary condition on the section is obtained by computing $S_{in}(t)$ such that $Q_{in}(t) = Q^{(0)}(S_{in}(t))$. The left boundary conditions on the enstrophy and potential are their respective zeroth-order asymptotic expansions. Finally, we consider homogeneous Neumann boundary conditions on the right boundary. Regarding the 2D code, the top and bottom boundaries are solid walls, and we prescribe standard 2D inflow and outflow boundary conditions at the left and right boundaries, respectively.

In Figure 8, we display the free surface H (left panels) and discharge Q (right panels) at dimensional times 2h (top panels) and 9h (bottom panels). The solid blue line with $\times$ marks represents the width-averaged 2D reference solution. The dashed line and the solid line with + marks respectively represent the results of the A0 and A1 models. The results of the kinematic waves approximation, labeled H^{KW} and $Q^{KW} = Q^{(0)}(H^{KW})$, are represented with dotted lines. On each panel, we magnify the point where the differences between the four models are the largest. The magnification level for each panel is written under the line connecting the magnifying glass to the graphs.

We consistently observe that the A1 model yields the best approximation of the 2D reference solution, as expected since it recovers the first-order expansion of the discharge. The approximation obtained with the KW model is worse than the one coming from the A0 model, even if both recover the zeroth-order expansion $Q^{(0)}$ of the discharge. The most striking differences between the models are located where the flood advances on the steady river. This denotes a difference between the zeroth-order and first-order friction models.

To get a better understanding of the relevance of the A1 model compared to the A0 one, we now display in Figure 9 the relative errors in space between the 2D reference solution and the models with respect to the dimensional time. The relative spatial errors in L^2 norm are computed as follows:

$$\left\| \frac{H^{A1}(\cdot,t) - H^{2D}(\cdot,t)}{H^{2D}(\cdot,t)} \right\|_{L^2} = \sqrt{\int_{\xi_1} \left| \frac{H^{A1}(\xi_1,t) - H^{2D}(\xi_1,t)}{H^{2D}(\xi_1,t)} \right|^2 d\xi_1},$$

and the relative spatial errors in L^∞ norm as defined by:

$$\left\| \frac{H^{A1}(\cdot,t) - H^{2D}(\cdot,t)}{H^{2D}(\cdot,t)} \right\|_{L^\infty} = \max_{\xi_1} \left| \frac{H^{A1}(\xi_1,t) - H^{2D}(\xi_1,t)}{H^{2D}(\xi_1,t)} \right|.$$

In the left panel of Figure 9, we display the errors in L^2 norm, and we display the errors in L^∞ norm in its right panel. The errors made by the KW, A0 and A1 models are respectively depicted with dotted lines, dashed lines and solid lines.

We observe, like in Figure 8, that the KW model produces a worse approximation than the A0 model, whose approximation is itself worse than the one given by A1 model. Indeed, the maximum over time of the spatial error in L^2 norm is around 23.6% for the KW model, 11.3% for the A0 model and 3.17% for the A1 model. The maximum over time of the spatial error in L^∞ norm is around 22.6% for the KW model, 14.0%

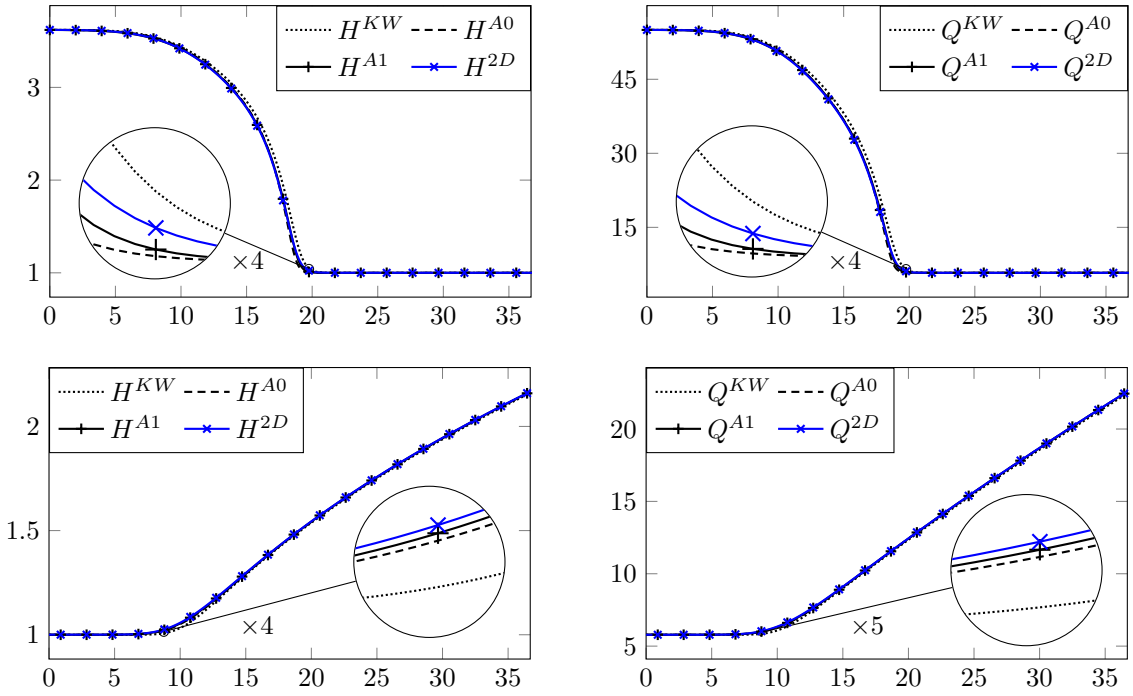

Figure 8: Free surface H (left panels) and discharge Q (right panels) for the flood experiment. Comparison of the 2D reference solution with the A0 and A1 models, as well as the kinematic waves (KW) approximation. The results are displayed with respect to the position, at dimensional times $t = 2$h (top panels) and $t = 9$h (bottom panels). Magnification of the zones where the three models yield the most different results, with magnification level written below the line linking the magnifying glass to the graphs.

for the A0 model and 3.81% for the A1 model. Once again, the advantages of the A1 model over the other two models are undeniable. Note that similar conclusions can be obtained from the study of the discharge errors, and we do not display the error curves here for the sake of conciseness.

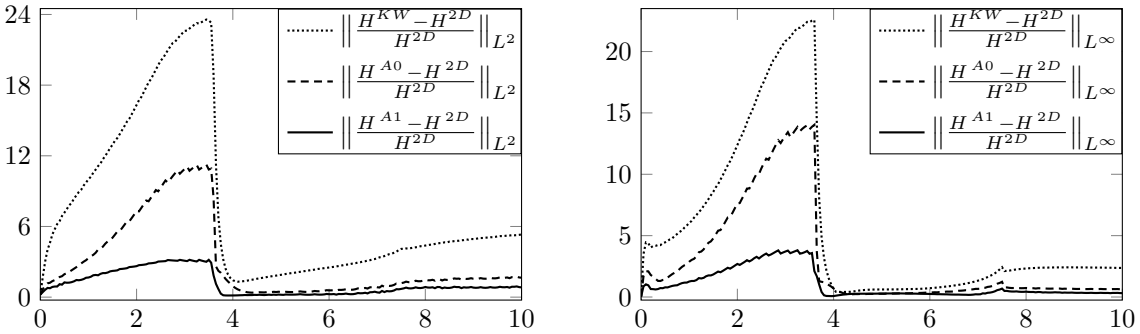

Figure 9: Relative errors in space in L^2 norm (left panel) and in L^∞ norm (right panel) between the 2D reference solution and the KW model (dotted lines), the A0 model (dashed lines) and the A1 model (solid lines), represented with respect to the dimensional time.

In the left panels of Figure 10, we display the relative errors between the reference solution and the models, with respect to time and at the probe located at $\xi_1 \simeq 34.57$. The top left panel displays the error on H while

the bottom left panel displays the error on Q. The errors between the 2D reference solution and the A0 and A1 models are respectively represented with a dashed line and a solid line. In the right panels, we display a zoom around the point $\xi_1 \simeq 34.57$ at dimensional time 3.35h, when the errors are the largest. The top right panel displays H and the bottom right one displays Q. The color coding is the same as in Figure 8.

The observations we had made in Figure 8 are confirmed by Figure 10. Indeed, at the probe, the largest difference in free surface H are around 11.9% for the A0 model and 2.00% for the A1 model. Regarding the discharge Q, the largest differences at the probe are about 25.9% for the A0 model and 4.86% for the A1 model. These differences are obtained around dimensional time 3.35h, when the peak of the advancing flood reaches the probe at $\xi_1 \simeq 34.57$. Note that the differences between the reference solution and the zeroth-order models are closely related to the values of $\frac{\varepsilon F^2}{J_0} \simeq 0.175$ and $(\frac{\varepsilon F^2}{J_0})^2 \simeq 3.06 \times 10^{-2}$.

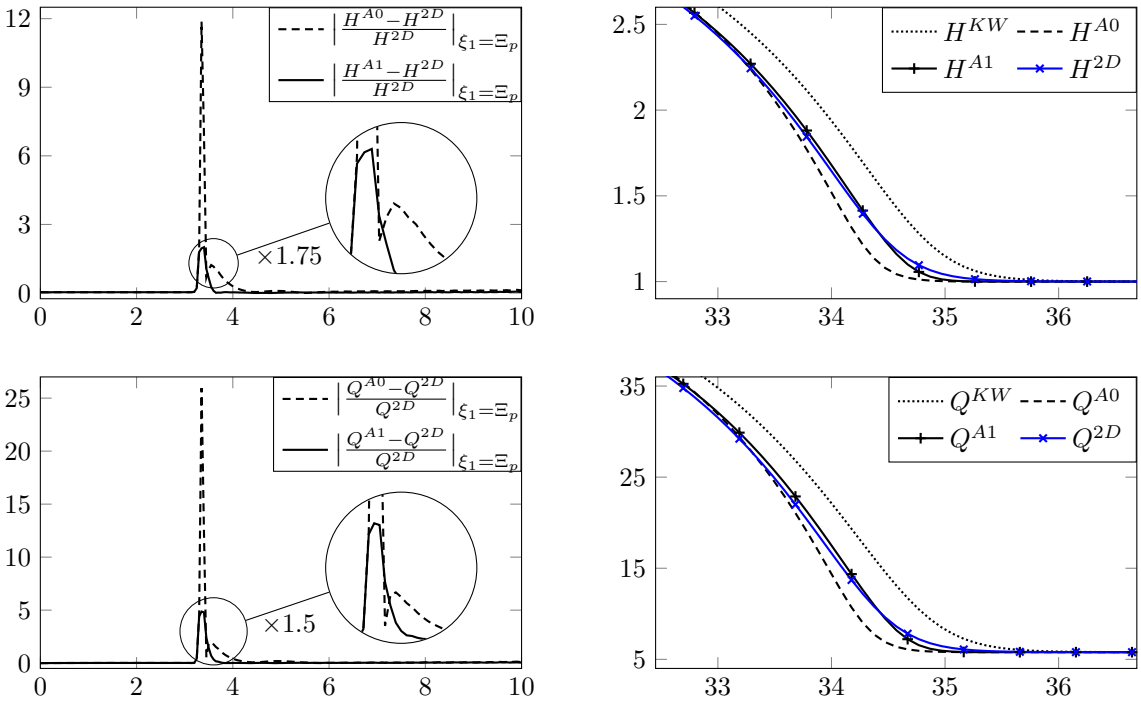

Figure 10: Left panels: relative errors between the 2D reference solution and the A0 and A1 models (the dashed line for the A0 model and the solid line for the A1 model). The errors on H are displayed in the top left panel and the ones on Q are depicted in the bottom left panel. These errors are computed at non-dimensional position $\xi_1 \simeq 34.57$ and are plotted with respect to the dimensional time. Right panels: free surface H (on top) and discharge Q (at the bottom) for the flood experiment, computed with the 2D system as well as the A0 and A1 models, and displayed with respect to the position, at dimensional time 3.35h. Magnification of the zones where the three models yield the most different results, with magnification level written below the line linking the magnifying glass to the graphs.

Acknowledgments. The authors extend their thanks to the Service d'Hydrographie et d'Océanographie de la Marine (SHOM) for financial support. The authors would like to warmly thank Frédéric Couderc for his help in setting up the DASSFLOW flood experiment.

References

[Bispen et al., 2014] Bispen, G., Arun, K. R., Lukáčová-Medviďová, M., and Noelle, S. (2014). IMEX large time step finite volume methods for low Froude number shallow water flows. *Commun. Comput. Phys.*, 16(2):307–347.

[Bresch and Noble, 2007] Bresch, D. and Noble, P. (2007). Mathematical Justification of a Shallow Water Model. *Methods and Applications of Analysis*, 14(2):87–118.

[Chen and Duan, 2006] Chen, D. and Duan, J. (2006). Modeling width adjustment in meandering channels. *Journal of Hydrology*, 321(1-4):59–76.

[Couderc et al., 2015] Couderc, F., Madec, R., Monnier, J., and Vila, J.-P. (2015). *DassFlow v2.00.00 : User and Developer Guide*. CNRS / IMT / INSA Toulouse / UPS, http://www.math.univ-toulouse.fr/DassFlow.

[Dammuller et al., 1989] Dammuller, D. C., Bhallamudi, S. M., and Chaudhry, M. H. (1989). Modeling of Unsteady Flow in Curved Channel. *J. Hydraul. Eng.*, 115(11):1479–1495.

[Decoene et al., 2009] Decoene, A., Bonaventura, L., Miglio, E., and Saleri, F. (2009). Asymptotic derivation of the section-averaged shallow water equations for natural river hydraulics. *Math. Models Methods Appl. Sci.*, 19(03):387–417.

[Fernández-Nieto et al., 2010] Fernández-Nieto, E., Marin, J., and Monnier, J. (2010). Coupling superposed 1D and 2D shallow-water models: Source terms in finite volume schemes. *Comput. & Fluids*, 39(6):1070–1082.

[LeVeque, 2007] LeVeque, R. J. (2007). *Finite Difference Methods for Ordinary and Partial Differential Equations: Steady-State and Time-dependent Problems (Classics in Applied Mathematics)*. Society for Industrial and Applied Mathematics.

[Luchini and Charru, 2010] Luchini, P. and Charru, F. (2010). Consistent section-averaged equations of quasi-one-dimensional laminar flow. *J. Fluid Mech.*, 656:337–341.

[Marin and Monnier, 2009] Marin, J. and Monnier, J. (2009). Superposition of local zoom models and simultaneous calibration for 1D–2D shallow water flows. *Math. Comput. Simul*, 80(3):547–560.

[Monnier et al., 2016] Monnier, J., Couderc, F., Dartus, D., Larnier, K., Madec, R., and Vila, J.-P. (2016). Inverse algorithms for 2D shallow water equations in presence of wet dry fronts: Application to flood plain dynamics. *Adv. Water Resour.*, 97:11–24.

[Odgaard, 1989a] Odgaard, A. J. (1989a). River-Meander Model. I: Development. *J. Hydraul. Eng.*, 115(11):1433–1450.

[Odgaard, 1989b] Odgaard, A. J. (1989b). River-Meander Model. II: Applications. *J. Hydraul. Eng.*, 115(11):1451–1464.

[Richard and Gavrilyuk, 2012] Richard, G. L. and Gavrilyuk, S. L. (2012). A new model of roll waves: comparison with Brock's experiments. *J. Fluid Mech.*, 698:374–405.

[Richard et al., 2017] Richard, G. L., Rambaud, A., and Vila, J.-P. (2017). Consistent equations for open-channel flows in the smooth turbulent regime with shearing effects. *J. Fluid Mech.*, 831:289–329.

[Zaghloul, 1998] Zaghloul, N. A. (1998). Hydraulic exponents M and N for gravity flow pipes. *Adv. Water Resour.*, 21(3):185–191.

[Zarrati et al., 2008] Zarrati, A. R., Jin, Y. C., and Karimpour, S. (2008). Semianalytical model for shear stress distribution in simple and compound open channels. *J. Hydraul. Eng.*, 134(2):205–215.